Ruslan Lagashkin

The Behaviour and Frequency-Dependent Parameters of the CNT-Covered Films in the Frequency Range of 50 MHz – 6.2 GHz

Helsinki Metropolia University of Applied Sciences

Degree of Electronics

Degree Programme of Technology

Thesis

30.05.2016

Helsinki Metropolia University of Applied Sciences

Author(s)	Ruslan Lagashkin
Title	The Behaviour and Frequency-Dependent Parameters of the CNT-Covered Films in the Frequency Range of 50MHz – 6.2GHz
Number of Pages Date	40 pages + 5 appendices 30 May 2016
Degree	Electronics
Degree Programme	Technology
Specialisation option	Nano and Radio Sciences
Instructor	Matti Fischer, Principal Lecturer

Theoretical basis for the frequency-dependent parameters measurement and calculation for the thin film conductive materials is described. The single layer and multilayer CNT-covered film disks were installed across the coaxial cable line and then short circuited. It was found that the resonant frequencies of the system are inversely proportional to the segment of the coaxial line length between the installed disks and the short circuiter. The resonant frequencies caused the attenuation due to the destructive interference up to -36dB. The Corbino disk reflectometry setup using a clutch device was used to measure the CNT-covered film complex load impedance Z_L at the frequencies of 50 MHz, 860 MHz, 2.45 GHz, 5 GHz and 6.2 GHz. Z_L was then used to calculate the film complex surface impedance Zs and the conductivity σ. The way to predict the thin film complex frequency-dependent surface impedance and surface impedance based on the DC Ω/□ measurement was found. The way to calculate most of the frequency-dependent thin film parameters based on the Z_L is described.

Keywords	CNT layer, thin film, Corbino disk, reflection coefficient, surface impedance, complex conductivity, frequency-dependent parameters

Contents

1 Introduction

The customer company specialises in the sphere of the conductive transparent CNT-covered films production.

The existing research indicates the possibility of the CNT-covered films use in the radio transmission [2, p.255-256] and electromagnetic radiation shielding [3, p.1-34] spheres.

Considering the transparency property of the manufactured conductive CNT-based materials, they could potentially be used to create the transparent high frequency transmitting and shielding applications.

To begin with, the specific frequency-dependent behaviour of the existing large-scale manufactured CNT-covered films in the widely used 50 MHz – 6.2 GHz band was not previously investigated, and the present work aims to cover this issue.

2 Theoretical Background

2.1 The Context of Topics

The role of the theoretical part is to explain the physical meaning and the relations of the vital frequency-dependent material parameters, justify the experimental setup and provide convenient ways to calculate the parameters from the measured data.

In the *Section 2.2*, the physical meaning of the permittivity and its relation to the conductivity is explained. The given relation allows to calculate one of the fundamental properties of the material, permittivity, from the known conductivity.

Sections 2.3 and *2.4* describe the properties of the electromagnetic waves, used as the test subjects during the process of the material parameters determination. *Section 2.4* gives the reason why it is possible to receive similar results from the large open-space measurements as well as from the much more compact in-coaxial line sample experiments.

Section 2.5 describes the relevant physics of the used coaxial transmission line, and provides the basis for the experiment boundary limitations.

Section 2.6 allows to calculate the material skin depth and can be used to demonstrate the differences between the metallic materials and the discussed material under test.

Section 2.7 explains the concept of the surface impedance which is then used in the further sections.

Section 2.8 states that the wave can be either transmitted, reflected or absorbed, which later provides the ground for interpretation of the measured results in terms of the shielding effectiveness.

Sections 2.9 – 2.12 provide the practical formulas for different parameters calculation from the Corbino ring experiment. The subject parameters of these sections uniquely define all the frequency-dependent parameters of the transmission medium, which can be then found by substituting the known values to the equations on the page 23 of the [4] and then used for the material simulation and high frequency applications design.

2.2 Permittivity and Conductivity Relation

The absolute permittivity is the measure of how much the medium opposes the formation of electric field within itself. It employs the phenomena of charge migration as well as rotation of dipole charge carrying parts, as illustrated by Figure 1:

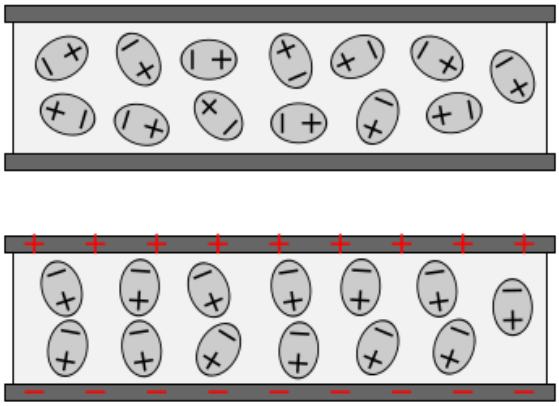

Figure 1. Reprinted from [5] *The reorientation of dipole particles in the presence of an electric field. The upper part of the figure shows the medium that consists of dipole particles in random orientation. In the lower part of the Figure, the same medium is treated with an external electric field denoted by + and – symbols. The dipole particles rotate and align parallel to the lines of electric field.*

Naming the described charge carrying particles displacement and reorientation as the dielectric displacement field D, in the presence of the electric field E, the scalar electric permittivity ε would be the relation coefficient between them:

(1)

$$D = \varepsilon \mathrm{E}$$

Where

- D is the dielectric displacement field in medium
- E is the external electric field
- ε is the DC permittivity

The permittivity can be scalar or complex, in anisotropic medium it is a second rank tensor. It depends on temperature, pressure and structure. [6, p.2]

The complex permittivity depends on frequency [6, p.2]. It is the ratio between the vector alternating electric field E(ω) and the vector polarization P(ω):

(2)

$$P(\omega) = (\varepsilon^*(\omega) - 1)\varepsilon_0 E(\omega)$$

Where

- P(ω) is the vector polarization in medium
- ε*(ω) is the complex dielectric constant
- ε_0 is the permittivity of free space
- E(ω) is the electric field at the certain frequency

The components of complex permittivity ε* will be denoted as ε' for real part and ε'' for the imaginary part:

(3)

$$\varepsilon^* = \varepsilon' + \mathrm{j}\varepsilon''$$

The components of the complex permittivity ε* have the direct physical interpretation. Thus, the ε' is related to the energy stored reversible in material, and ε'' is related to the energy which is dissipated per cycle [6, p.2].

The relation between the frequency dependent permittivity and the frequency dependent conductivity is described in the equation (4) [6, p.2]:

(4)

$$\sigma^*(\omega) = i\omega\varepsilon^*(\omega)$$

Where

- σ* is the complex conductivity
- ω is the angular frequency

2.3 Impedance of Free Space and of Dielectric Medium

The impedance of free space Z_0 describes the relation between the electric and magnetic field vector magnitudes of the radiation travelling through the vacuum:

(5)

$$Z_0 = \frac{|E|}{|H|}$$

Where

- Z_0 is the impedance of free space
- |E| is the magnitude of the electric field
- |H| is the magnitude of the magnetic field

The value of the impedance of free space is calculated from the equation (6) [4, p.227]:

(6)

$$Z_0 = \left(\frac{L_1}{C_1}\right)^{1/2} = \frac{4\pi}{c} = 377\Omega$$

Where

- L_1/C_1 equals the ratio μ_0/ε_0
- c is the speed of light

In case the wave propagates in a dielectric medium with impedance $\dot{Z}_c$ it depends on the medium complex dielectric constant έ and magnetic constant μ_1 [4, p.227]:

(7)

$$\dot{Z}_c = Z_0 \left(\frac{\mu_1}{\acute{\varepsilon}}\right)^{1/2}$$

Where

- $\dot{Z}_c$ is the characteristic impedance of the medium
- μ_1 is the magnetic constant of free space
- έ is the complex dielectric constant

The losses depend on the imaginary part of έ and with its larger values can become significant [4, p.227].

2.4 TEM Waves

The transverse electric and magnetic waves, TEM waves have both electric and magnetic components of the travelling electromagnetic field perpendicular to the direction of travel:

(8)

$$E_{longitudinal} = H_{longitudinal} = 0$$

Where

- $E_{longitudinal}$ is the electric field component in the direction of propagation
- $H_{longitudinal}$ is the magnetic field component in the direction of propagation

The characteristic impedance of a TEM wave $\dot{Z}_{TEM}$ is given by the equation (9) [4, p.221]:

(9)

$$\dot{Z}_{TEM} = \frac{4\pi}{c}\left(\frac{\mu'_1}{\varepsilon'_1}\right) = Z_0\left(\frac{\mu'_1}{\varepsilon'_1}\right)^{1/2}$$

Where

- Z_{TEM} is the characteristic impedance of the transverse electromagnetic wave
- μ'_1 and ε'_1 are the real parts of the magnetic and electric constants of the transmission line

In the free space only the TEM waves propagate. Guiding structures with more than one conductor support the TEM wave propagation. In coaxial cables, the travelling transverse electric filed is radial, as illustrated by the Figure 2, and the transverse magnetic field is circular. [4, p.222]

2.5 Coaxial Cable

2.5.1 Geometric Coefficient

The geometric coefficient of a coaxial cable is based on the physical dimensions of its inner and outer conductor as shown in Figure 2:

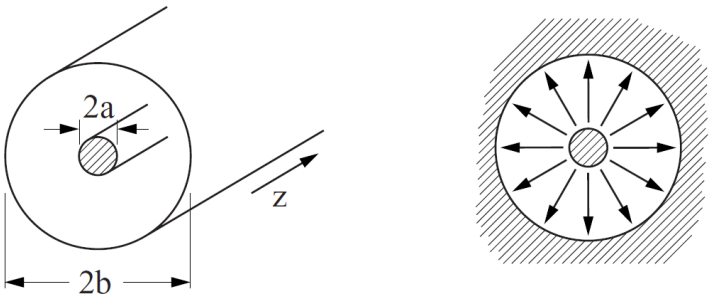

Figure 2 Reprinted from [4]*(225). On the left side is the schematic representation of the coaxial cable, with a being the radius of the inner conductor and b is the radius of the outer conductor. z is the length of the cable. On the right side – the representation of the electric field propagation in coaxial lines.*

The coaxial cable geometric coefficient G is provided by the equation based on the relation between outer and inner conductor radius [4, p.228]:

(10)

$$G = \frac{1}{2\pi}\ln\left(\frac{b}{a}\right)$$

Where

- a is the inner conductor radius
- b is the outer conductor radius

2.5.2 Characteristic Impedance

The characteristic impedance Z_c of the coaxial cable, which is generally the characteristic impedance of the plane wave $\dot{Z}_{TEM}$ multiplied with the geometric coefficient G [4, p.229]:

(11)

$$Z_c = Z_0 \left(\frac{\mu'_1}{\varepsilon'_1}\right)^{1/2} \frac{1}{2\pi} \ln\left(\frac{b}{a}\right)$$

Where

- Z_c is the characteristic impedance
- μ'_1 and ε'_1 are the real parts of the magnetic and electric constants of the transmission line

Since the coaxial cable characteristic impedance Z_c depends on the ration between the outer and inner radiuses, that means that a coaxial cable of a given impedance can have any absolute diameter.

2.5.3 Frequency Limitation

The higher frequency limitation for the coaxial line due to the increasing resistance per unit length R_1 follows from the equation (12) [4, p.229]:

(12)

$$R_1 = \frac{4\pi}{c}\left(\frac{f}{\sigma_1}\right)^{\frac{1}{2}} \frac{1}{4\pi}\left(\frac{1}{a} + \frac{1}{b}\right)$$

Where

- R_1 is the resistance per unit length of the coaxial cable
- f is frequency
- σ_1 is the complex conductivity

2.6 Skin Depth

The notation for components of the complex conductivity σ* will be as in the equation (13):

(13)

$$\sigma^* = \sigma_1 + j\sigma_2$$

Where

- σ* is the complex conductivity
- σ_1 is the real part of the complex conductivity
- σ_2 is the complex part of the complex conductivity

The skin depth δ which is defined as a distance over which the incident electromagnetic radiation attenuates by the factor 1/e, is given by the equation (14) [4, p.25]:

(14)

$$\delta = \frac{c}{\omega k} = \frac{c}{\sqrt{2\pi\omega\mu_1}\sqrt{\sqrt{{\sigma_1}^2 + {\sigma_2}^2} + \sigma_2}}$$

Where

- k is the extinction coefficient of the electromagnetic wave travelling into medium
- μ_1 is the real part of the magnetic constant of the medium

If the amplitudes of the real part of the conductivity is much bigger then the complex conductivity part, e.g. $\sigma_1 >> \sigma_2$ which is a natural situation for metals, then the skin depth δ_{metal} can be simplified to the equation (15):

(15)

$$\delta = \frac{c}{\sqrt{2\pi\omega\mu_1\sigma_1}}$$

The power absorption coefficient α is the power absorbed in the unit volume [4, p.28] is described by the equation (16):

(16)

$$\alpha = \frac{2}{\delta}$$

Where

- α is the absorption coefficient
- δ is the conductivity

2.7 Surface Impedance

Consider the complex surface impedance $\dot{Z}_s$ which is the ratio between the normal of the electric field to the surface and all the total current density induced in the material [4, p.42]. The real part of $\dot{Z}_s$ is responsible for the power absorption, while the imaginary part

is causing the phase shift. The definition and the general form of the surface impedance is given in the equation (17) [4, p.42]:

(17)

$$\dot{Z}_s = \frac{\hat{E}_{z=+0}}{\int_0^\infty \hat{J}\, dz} = R_s + jX_s$$

Where

- $\dot{Z}_s$ is the surface impedance or impedance of the wave
- $\hat{E}_z$ is the normal of the electric field to the surface, vector quantity
- $\hat{J}$ is the induced current in the direction of z
- R_s is the real part of the impedance
- X_s is the imaginary part of the impedance

2.8 Reflectivity and Absorptivity

The reflectivity in terms of $\dot{Z}_s$ is then given by the ratio in the equation (18):

(18)

$$R = \left| \frac{\dot{Z}_s - \dot{Z}'_s}{\dot{Z}_s + \dot{Z}'_s} \right|^2$$

Where

- $\dot{Z}'s$ is the prime medium impedance the wave is travelling from

The wave can be reflected, transmitted or absorbed:

(19)

$$R + T + A = 1$$

Where

- R is the reflectivity
- T is the transmissivity
- A is the absorptivity

2.9 Complex Reflection Coefficient S_{11} from Load Impedance

The impedance mismatch in the transmission medium causes some part of the wave to be reflected. The complex reflection coefficient denoted in this work as S_{11} is the ratio between the electric filed strength of the reflected wave $E_{reflected}$ to the electric field strength of the incident wave $E_{incident}$:

(20)

$$S_{11} = \frac{E_{reflected}}{E_{incident}}$$

Where

- S_{11} is the reflection coefficient, dimensionless
- $E_{reflected}$ is the reflected wave electric field strength
- $E_{incident}$ is the incident wave electric field strength

The complex reflection coefficient S_{11} can be found from the complex load impedance Ż by using the equation (21) [4, p.232]:

(21)

$$S_{11} = \frac{\dot{Z}_L - \dot{Z}_S}{\dot{Z}_L + \dot{Z}_S}$$

The return loss RL is a common decibel measure of the reflected wave and relates to the reflection coefficient by the terms of equation (22):

(22)

$$RL = -20log_{10}\left(\frac{1}{|S_{11}|}\right)$$

Where

- RL is the return loss, measured in [dB]
- $|S_{11}|$ is the magnitude of the reflection coefficient

2.10 Conductivity from S_{11}

The load impedance Z_L of the sample under test, terminated by a highly conductive material, can be found with the complex reflection coefficient S_{11}, as shown in the equation (23) [7, p.2]:

(23)

$$Z_L = Z_c \frac{1 + S_{11}}{1 - S_{11}}$$

Where

- Z_L is the load impedance of the sample at the end of the cable
- Z_c is the characteristic impedance of a coaxial cable
- S_{11} is the complex reflection coefficient

In highly conductive films, the surface impedance Z_s relates to the load impedance Z_L as shown in the equation (24) [7, p.2]:

(24)

$$Z_L = GZ_s\coth(kt)$$

Where

- G is the geometry coefficient of a coaxial cable
- Z_s is the surface impedance
- k is the complex propagation constant
- t is the material thickness

In the condition of the magnitude of the complex skin depth δ being much bigger than the material thickness t, the coth(kt) can be approximated to 1/kt [7, p.2], leading to the equation (25):

(25)

$$Z_L \approx \frac{GZ_s}{kt}$$

At the same time, the ratio between the surface impedance Zs and the propagation constant k can be simplified using the representation from the local electrodynamics [7, p.2]:

(26)

$$\frac{Z_s}{k} = \frac{\sqrt{\frac{i\mu_0\omega}{\sigma}}}{\sqrt{i\mu_0\omega\sigma}} = \frac{1}{\sigma} \Rightarrow$$

Where

- μ_0 is the permeability of free space
- ω is the angular frequency
- σ is the conductivity

(27)

$$Z_L \approx \frac{G}{\sigma t}$$

In case of primary medium being air and corresponding $Z' = Z_0$ and $\mu'_1 \approx \varepsilon'_1 \approx 1$, the conductivity σ can be expressed as in the equation (30):

(28)

$$\sigma = \frac{G}{Z_L t}$$

(29)

$$\sigma = \frac{G}{Z_c t}\left(\frac{1+S_{11}}{1-S_{11}}\right)^{-1}$$

(30)

$$\sigma = \frac{1}{Z_0 t}\left(\frac{1 - S_{11}}{1 + S_{11}}\right)$$

Where

- Z_0 is the characteristic impedance of free space

2.11 Surface Impedance from S_{11}

The geometry coefficients of the coaxial cable and the Corbino disk cancel each other and the formula for the surface impedance Z_s is derived to the equation (31):

(31)

$$Z_s = \dot{Z}_{TEM} \times \left(\frac{1 + S_{11}}{1 - S_{11}}\right)$$

Where

- Z_s is the material under test surface impedance
- S_{11} is the complex reflection coefficient

The form that may be more handy in the practical applications is derived by expanding the TEM wave impedance into the transmission line impedance and the coaxial cable geometry coefficient, as shown in the equation (32) [8, p.2]:

(32)

$$Z_s = Z_c \frac{2\pi}{\ln\left(\frac{b}{a}\right)}\left(\frac{1 + S_{11}}{1 - S_{11}}\right)$$

Where

- Z_c is the characteristic impedance of the coaxial transmission line
- a and b are the inner and outer diameter of a coaxial cable

2.12 Complex Propagation Constant from Conductivity

The complex propagation constant γ as the complex quantity can be written in the form of equation (33):

(33)

$$\gamma = \alpha + j\beta$$

Where

- γ is the complex propagation constant
- α is the real part of the propagation constant
- β is the complex part of the propagation constant

γ is derived from the conductivity by the equation (34) [7, 2]:

(34)

$$\gamma = \sqrt{i\omega\mu_0\sigma}$$

Where

- ω is the angular frequency
- μ_0 is the permeability of free space
- σ is the conductivity

3 Methods and Materials

3.1 CNT-Covered Films

The material under test (MUT) is manufactured by the customer company with the proprietary technology. In general, MUT consists of the polyethylene terephthalate (PET) substrate covered with the layer of the carbon nanotube (CNT)-based material.

The CNT-based layer thickness is inversely proportional to the complex frequency-dependent conductivity (the thicker the layer, the less conductive it needs to be for the same output). For the calculations in this work, the thickness of the CNT-based layer is taken as 100 nm.

The PET substrate thickness does not affect the DC resistance, but may affect the frequency-related CNT-based layer parameters measurements, if it is more than 0.1 compared to the quarter wavelength of the test frequency. In the context of this work, the highest test frequency was 13.5 GHz with the corresponding quarter wavelength in free space of 5.5 mm, which is considerably longer than the substrate layer thickness.

3.2 4-wire Ω/□ Measurement

The 4-wire Kelvin measurement is used for the precise resistance measurement and allows to get rid of the internal resistance of the measuring wires. In the case of 2D electronics, it allows to avoid the strong connection point resistance contribution, Figure 3:

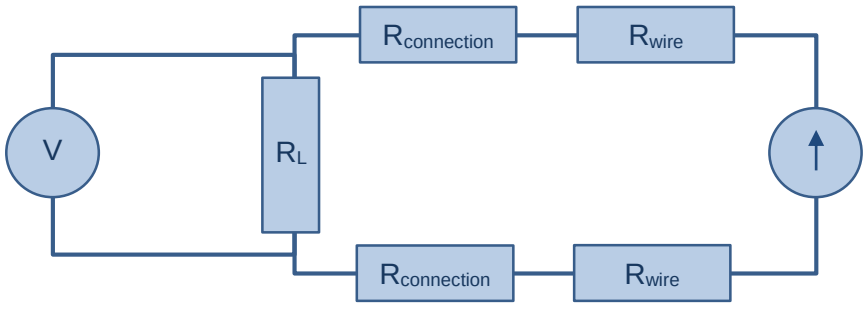

Figure 3. 4-wire resistance measurement. From the right: the known current source drives the current through the probe wires, probe - 2D film connection points and the load resistance R_L. The voltmeter is connected across the R_L, thus measuring the voltage drop due to the known current stream.

For the 2D films, the resistance is obtained in the form of ohms per square, [Ω/□]. The square comes from the fact that the resistance is directly proportional to the rectangular sample length and inversely proportional to the rectangular sample width, thus the 2D conductive square od arbitrary size made out of the same material, would have the same side-to-side resistance.

The Jandel RM3-AR combined constant current source and digital voltmeter was used for the DC resistance measurement.

3.3 Network Analyser

During the CNT-covered film disk in coaxial cable experiment and the Corbino disk reflectometry experiment, the Hewlett Packard 8719ES 50 MHz to 13.5 GHz S-Parameter Vector Network Analyzer was used.

3.4 CNT-Covered Film Disk in Coaxial Cable

Since the coaxial cable guides the waves in TEM mode which is similar to the TEM wave propagation in free space, it is possible to model the covering of an object with the CNT-based material using the compact in-coaxial line setup.

The principle schematic of the CNT-covered film disk reflectometry experiment setup is shown in Figure 4:

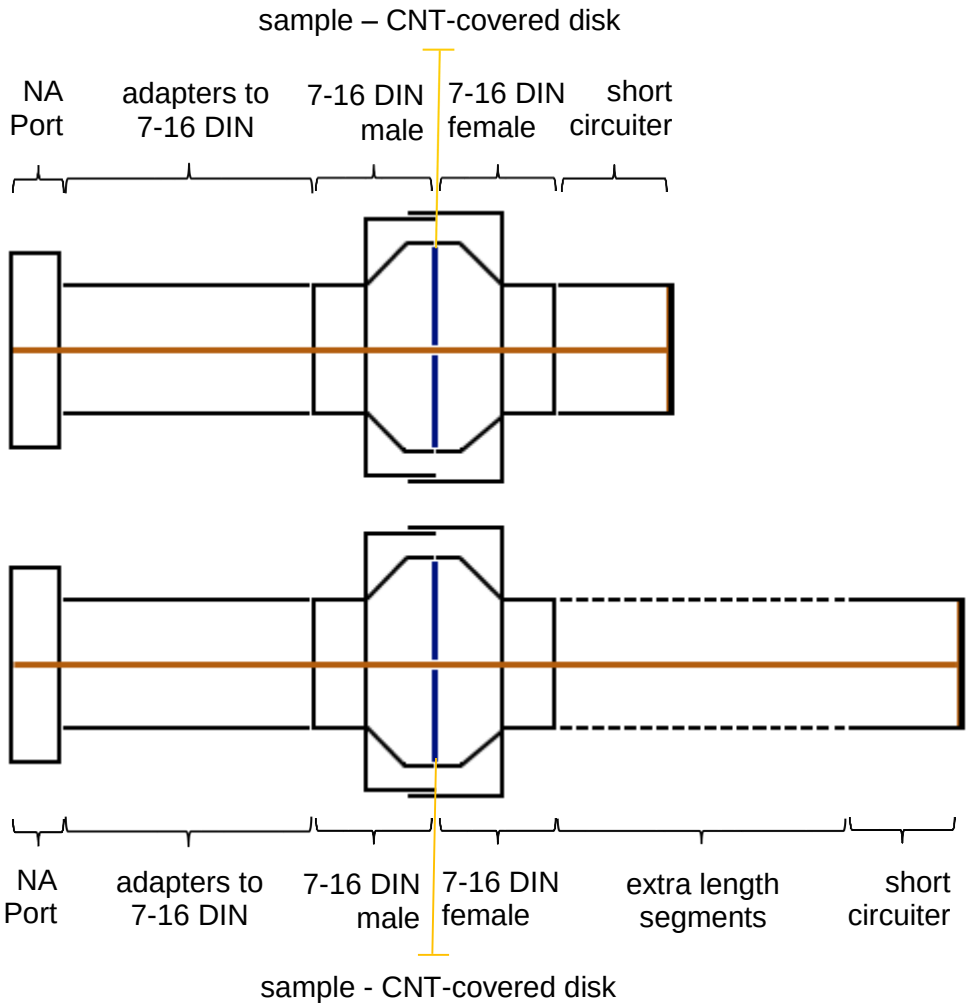

Figure 4. The principle schematic of the CNT-covered disk tab experiment. The largest available 7-16 DIN connector with the CNT-covered sample inside is connected to the network analyzer port from one side and short circuited from another. The distance between the sample and the short circuiter is varied using the additional coaxial line segments.

In half of the cases, the short-circuiter was off and the line was open circuit. This change results in a π phase shift of the reflected wave.

The sample is a thin disk with a cut out center that was placed across the coaxial cable, parallel to the propagating plane wave (Figure 2). The inner coaxial conductor goes through the center of the disk.

The 7-16 DIN connector was the thickest available coaxial connector with the outer conductor diameter of 16 mm and the inner of 7 mm. The CNT-covered disk installed in the cable was cut to fit into 7-16 DIN connector just barely, Figure 5:

Figure 5. On the right side is the 7-16 male connector. On the left side is the sandwich assembly - the foam in the middle and CNT-covered disks on bottom and top.

In the experiment, the CNT-covered disks were stacked from one side of the foam.

All together, the coaxial cable with the CNT-covered disk inside was connected to the network analyzer from one side and the short circuiter from another, Figure 6:

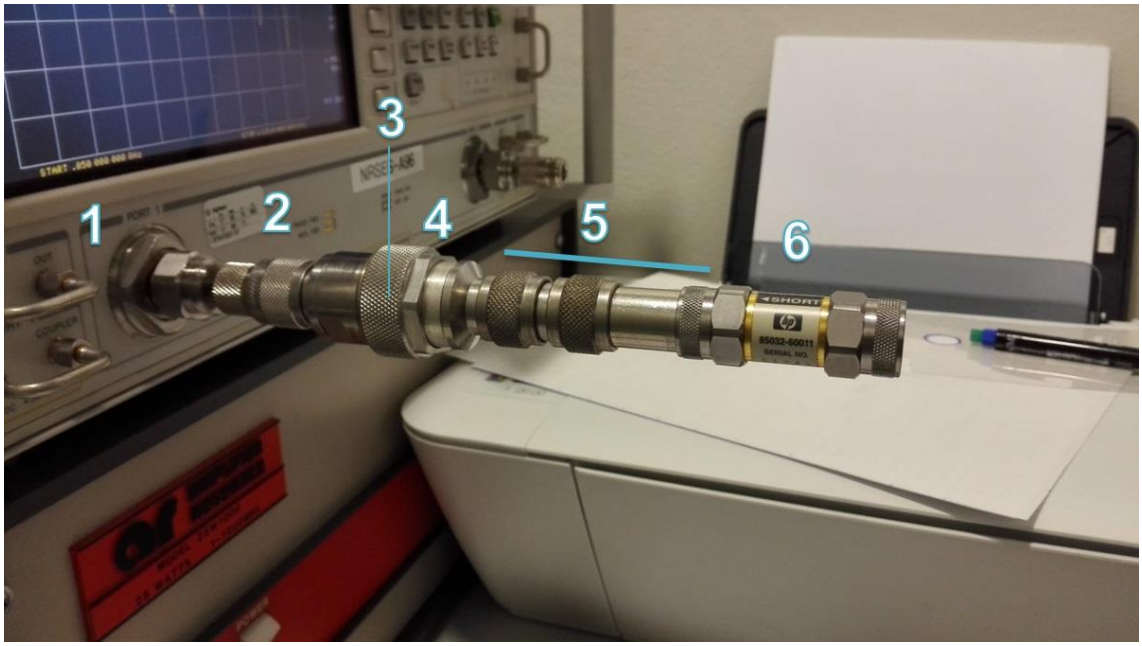

Figure 6. From the left hand side: (1) Network analyzer, (2) series of adapters to 7-16 DIN connector, (3) CNT-covered disk between connectors (not visible), (4) 7-16 DIN connector, (5) an extra segment made of N connectors, (6) short circuiter.

The network analyzer was set to port 1 reflection measurement mode. The default calibration coefficients of NA were used in this experiment and the reflection loss RL waveform was the output of this experimental setup.

3.5 Corbino Disk Reflectometry Setup

3.5.1 Principal Setup and Implementation

The principal Corbino disk reflectometry setup is shown in Figure 7:

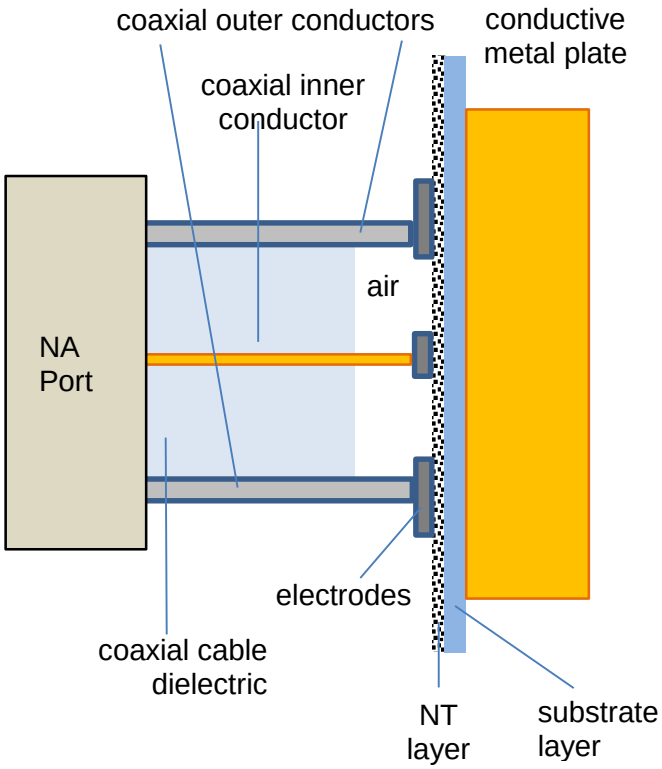

Figure 7. The network analyzer port is connected to the coaxial cable, which has inner and outer conductors and the dielectric layer between them. The conductors of the coaxial cable are connected to the sample through the electrodes to maintain the good connection to the NT layer. The NT layer of the sample is doped on the substrate layer. After the thin sample, the well conductive metal plate is located.

In order to maintain the good connection between the Corbino disk electrodes and the coaxial cable inner and outer conductors, the special clutch-based device was assembled, Figure 8:

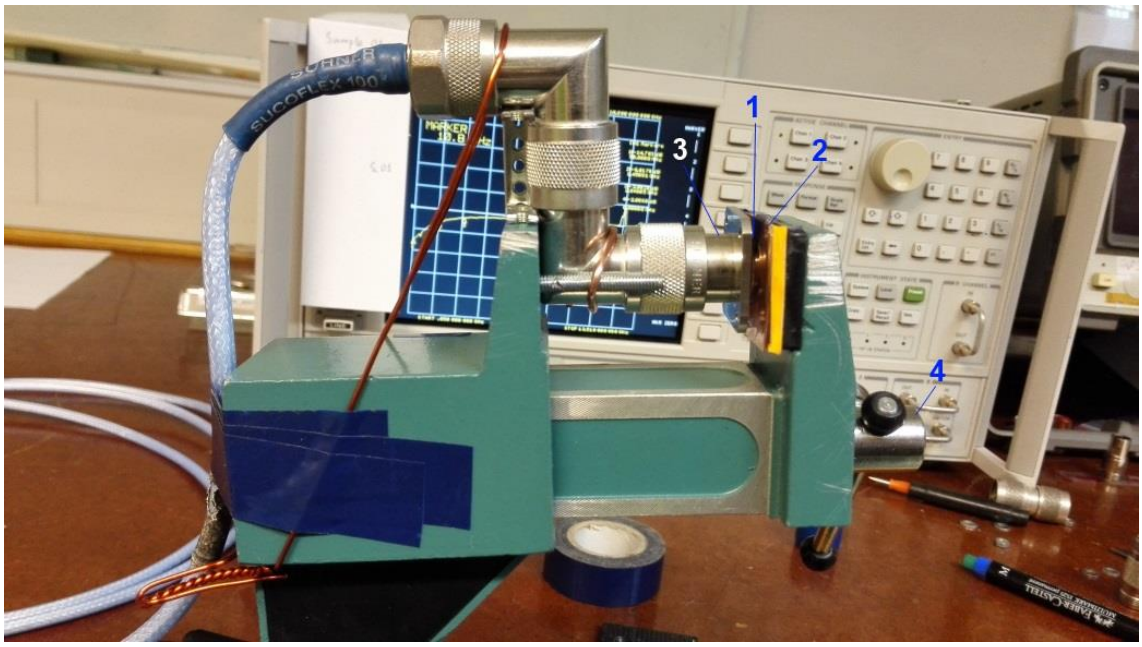

Figure 8. Pressing the sample to the coaxial cable conductors using clutch. The sample (1) is squeezed between the (2) copper reflective metal plate and the (3) modified type N panel mount adapter by tightening the clutch arm (4). The copper reflective metal plate has the rubber bed behind (yellow layer). The coaxial cable from the device is connected to the port of the network analyzer (on the background).

After the first calibration, the return loss RL for the target frequencies was measured. The raw measured data is summarized in Appendix 3. Since the RL waveform for each measurement within a single CNT-covered sheet was similar, waveform comparison of based on each sheet's 1st measurement of is located in Appendix 5.

After the second calibration, the complex load impedance Z_L, as well as the phase of the reflected signal for the target frequencies was measured. The raw measured data is summarized in Appendix 4.

3.5.2 Target Frequencies

The number of target frequencies was equal to the number of simultaneous markers in the used HP 8719ES network analyzer (NA). The following five frequencies were chosen:

- 50 MHz, since it was the lowest possible NA frequency
- 860 MHz, the European standard for the UHF RFID communication
- 2.45 GHz, the common Wi-Fi frequency
- 5 GHz, the second common Wi-Fi frequency

- 6.2 GHz or 6.9 GHz, the frequencies the unwanted resonance phenomena started to interfere with the MUT measurement data

The last frequency depended on the small geometry mismatches between the coaxial line end and the copper reflective plate. The resonance phenomena showed as a ‘loop’ in the Smith chart, or subsidence in the RL graph occurred. The location of the resonance was constant for the single assembly with same calibration. It was visible bot with the pure PET film installed as a sample and when the thin layer of air between the coaxial line conductors and the reflective plate was left. In any case, in order not to spoil the MUT data, the range was left out by setting the upper target frequency before it started.

3.5.3 End Point Calibration

The last coaxial line section of the clutch device was the type N male panel mount adapter.

Initially, the inner and outer conductors of the adapter were at the different distance from the end. Therefore, the end of the panel mount adapter was grinded and the protruding outer conductor was whittled away. This allowed to press the Corbino disk sample to the modified adapter and establish the good electrical connection to both outer and inner electrodes.

The length of the type N male panel mount adapter was 20 mm, Figure 9:

Figure 9. The length of the grinded type N panel mount adapter.

The measured 20 mm length of the adapter corresponded to the measured lengths of the calibration kit references - the short circuit in the short circuiter and the black something in the 50 Ω wideband reference. Therefore, the calibration was performed exactly at the point of the connection between the panel mount adapter and the Corbino ring disk samples.

For the two subsequent experiments, the last coaxial line segment of the clutch-based device was assembled and calibrated twice.

Preliminary to the first experiment, the device was calibrated at the point of sample connection with short and open circuiter. However, the calibration 50 Ω female wideband reference was connected only after the extra added male-to-male type N adapter.

The resonant frequency region after the first setup and calibration occurred to be in the region after 6.9 GHz. Therefore, 6.9 GHz was set to be the last target frequency.

Preliminary to the second experiment, the type N male 50 Ω wideband reference was found, and the device was calibrated at the point of sample connection with short circuiter, open circuiter and the 50 Ω wideband reference.

The second time, the resonant frequency region occurred after 6.2 GHz and, again, defined the upper target frequency.

3.5.4 Silver Paste Application and Curing

The electrodes for the Corbino disk were created by applying the layer of silver nano paste to the target areas.

The paste was applied using the stamping technique. The male-to-male type N adapter was used to stamp the outer conductor, and the 3 mm screw was used to stamp the inner Corbino disk conductor.

In addition to the stamping technique, several other ways to apply the silver paste to the CNT-covered films were tested. It is worth to mention that applying paste with smearing should be avoided, as it leads to the disruption of the NT layer. The silver paste printing,

on the other side, provides the best results in terms of the shape precision and the even thickness of the conductive layer.

The silver nano paste drying and solidifying process was taking more than 24 hours in a normal room conditions. In order to speed it up, the ultraviolet curing chamber was assembled, Figure 10:

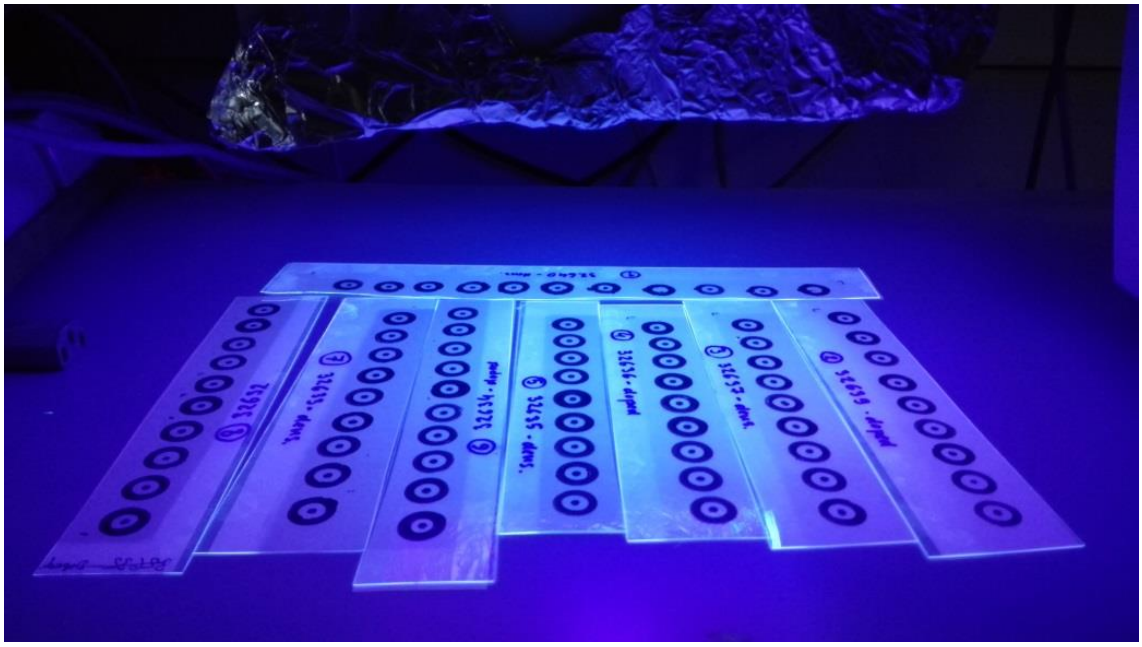

Figure 10, CNT-covered samples with applied silver paste (rings with dots in the middle) curing under the UV lamp. The radiation of the UV lamp is focused by the cardboard plafond covered with reflective aluminum foil.

The tests indicated that, under the curing chamber, it takes 40 minutes for the silver nano paste to solidify and become highly conductive. The samples under test (Figure 10) were irradiated by the UV light for over 12 hours.

3.5.5 Moving Sample Relative to Coaxial Cable

Since the precision of Corbino disk sample positioning in the clutch device was limited by the precision of the human hands, the experiment to estimate the magnitude of potential return loss deviations was performed.

At first, the sample was placed as centered as possible. Then, it was moved from the center by approximately 2mm, Figure 11:

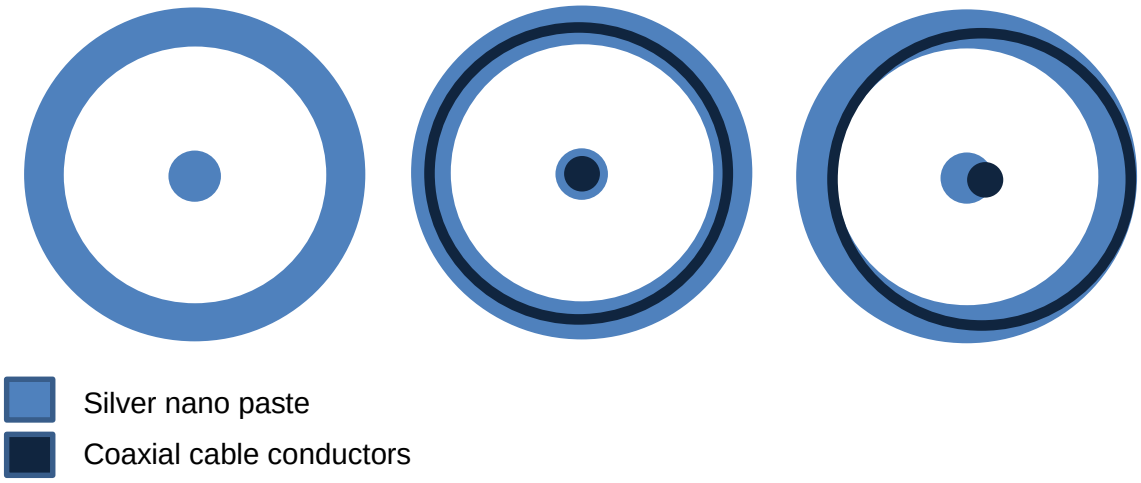

Figure 11. The modelling of the unwanted Corbino disk sample movement in respect to coaxial cable. On the left is the schematic representation of the Corbino disk electrodes made out of solidified silver paste. In the middle is the ideal situation, when the Corbino disk electrodes position is synchronized with the position of the coaxial cable conductors. On the right side is the situation when the sample is moved to the left and the outer conductor of the coaxial cable is barely touching the border of the Corbino disk electrode.

In each of the five positions (center, left, right, top, bottom), the associated reflection loss RL was measured and the deviations were compared with the deviations from the main measurements.

3.5.6 Data Processing

For the *first calibration* experiment, the chart from the raw measured return loss RL data was created. The chart is presented and analyzed in the 4.4.1 Results section.

For the *second calibration* experiment, the raw measured complex load impedance Z_L was used to calculate the MUT frequency-dependent surface impedance Z_S and the conductivity σ. The formulas from the 2.9, 2.10 and 2.11 Theoretical Background section were used in order to perform the calculations.

Z_S and σ were then fed into the trend curve fitting program and the resultant charts are demonstrated in the 4.4.2 and 4.4.3 Results sections.

3.5.7 Trend Curve Fitting Program

The function of the program that fits the best-fit curve through the number of data points is based on the implementation of the least-square method algorithm. For the 5 data points, the 4^{th} order polynomial curve was used. The text of the program is provided in the Appendix 3.

4 Results

4.1 4-Wire Ω/□ Measurement

The results for the MUT resistance per square 4-point measurement are summarized in the

Table 1:

sample number	Treatment	Sheet resistance (Ω/□)	stdev (%)
32632	**Doped**	105	3,6 %
32634	**Doped**	220	5,2 %
32636	**Doped**	449	4,5 %
32639	**Doped**	969	4,4 %
32633	Pristine	618	7,8 %
32635	Pristine	1077	8,3 %
32637	Pristine	2661	6,3 %
32640	Pristine	6505	9,0 %

Table 1. Resistance per square for the tested samples. Columns from left to the right: the unique code of the sample, the presence of extra materials in the CNT-based layer, the measured resistance, the standard deviation relative to the average value in percent.

As it can be seen from Table 1, the doped samples have generally lesser DC resistance compared to the pristine ones. The standard deviation for the resistance measurement is rather low and the data can be treated as reliable.

4.2 CNT-Covered Film Disk in Coaxial Cable Behaviour

4.2.1 Multilayer Reflection

In this section, the effects of placing a tab made out of one or several CNT-covered film layers as in the coaxial line will be investigated.

At first, one and two CNT-covered layers are used to make a tab disk. The resulting return loss RL waveform is shown in Figure 12:

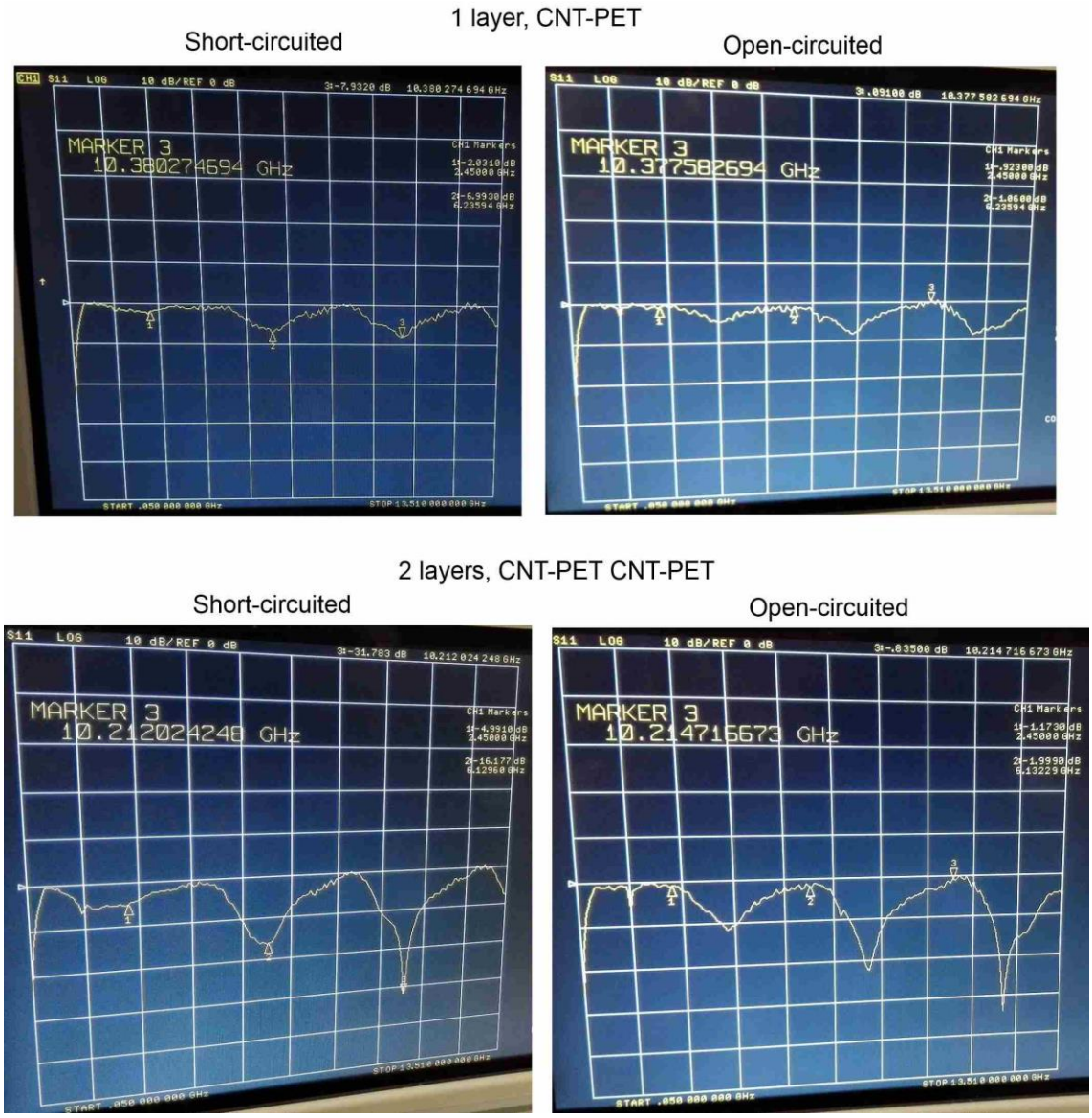

Figure 12 The upper two pictures show the RL after the single CNT-covered layer across the coaxial line. The lower two pictures show the effect of two layers. The left pictures describe the situation with the line short-circuited. The right pictures are the result of the open-circuited line. The maximum reflection is at the humps, and the minimum is at the dimples. The log vertical scale is used.

As it can be seen from Figure 12, installing the CNT-covered layer across the coaxial line as a tab, actually changes the amount of the reflected radiation compared to the “full reflection” 0 dB line in the middle of the screen. The maximum and minimum reflection frequencies seems to be inverted for the short and open-circuited line.

The addition of the second CNT-covered layer significantly increases the amount of not-reflected radiation at the resonant frequencies. The resonant frequencies, however, stay the same.

The different arrangement of 2 layer disks and comparison with the 3 layer disks is shown in

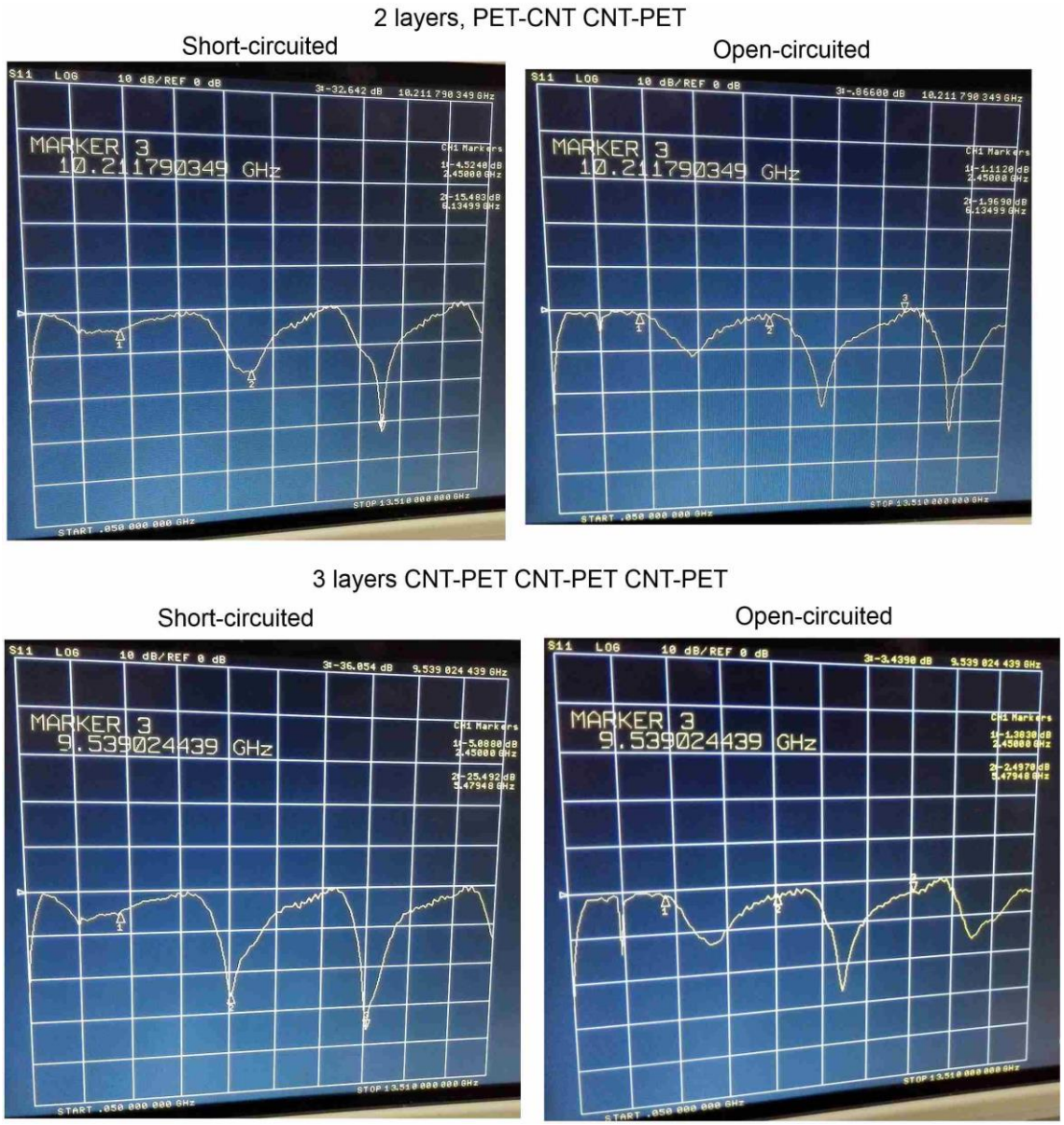

Figure 13. The 2-layer disk tab with the first disk flipped CNT to CNT way, the 3-layer disk tab.

As it can be seen from Figure 13, the dimples of the non-reflection become a bit deeper and the downward slopes are more acute. However, the thin anti-peaks can be a result of the superposition of the several anti-peaks and, considering their low quality, if the peaks eventually desynchronize, the acute anti-peaks vanish and resulting dimples of the non-reflection of the 3 layer disk tabs are even less than with 2 layers disk tabs (see

the last anti-peak of the right pictures in Figure 13). Another explanation is that the multilayer system is physically thicker and works better on the lower frequencies with longer wavelengths. This position is enforced by the data from the 4-layer system measurements, Figure 14:

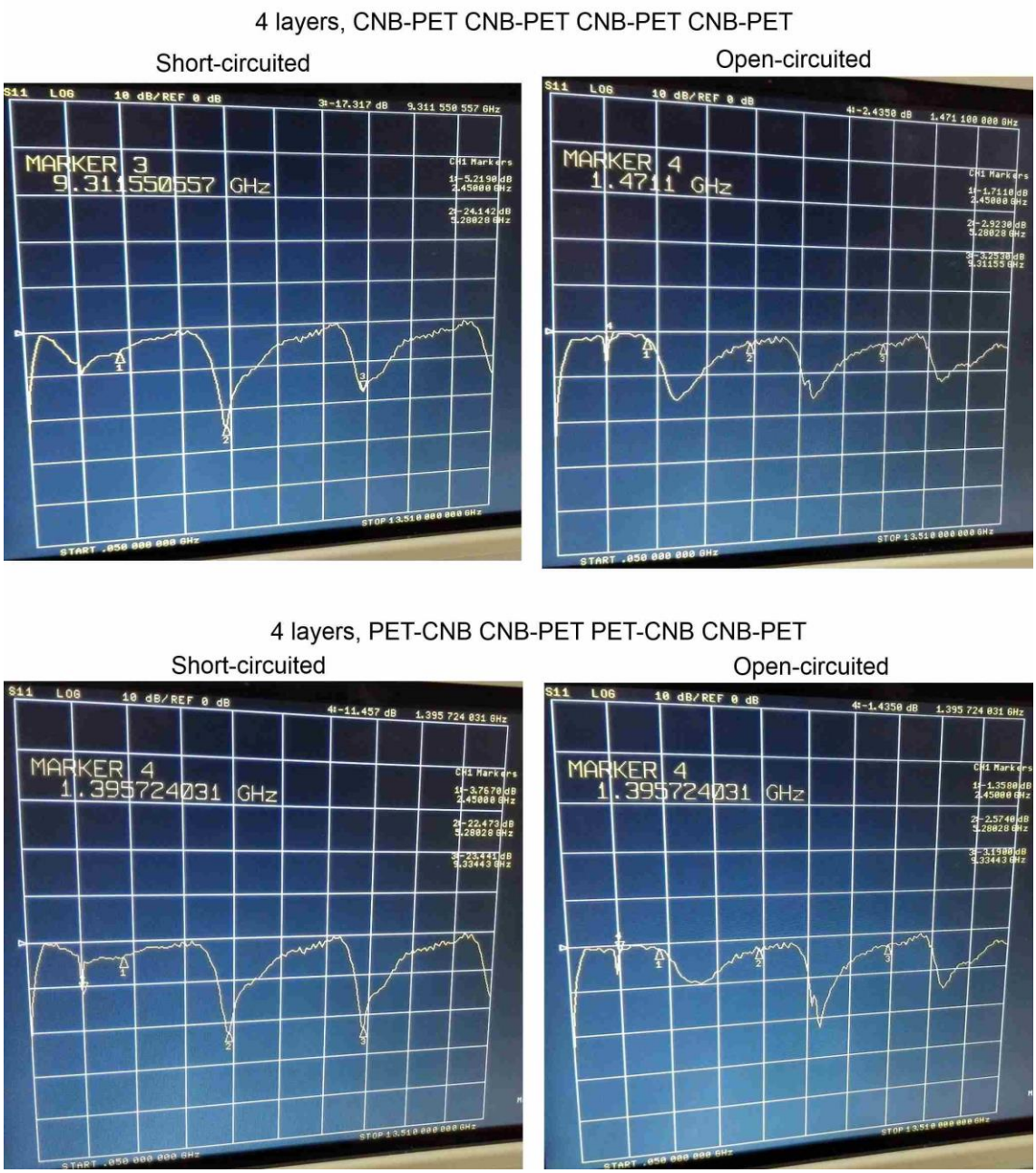

Figure 14 The 4 layers disk tabs in coaxial line in different arrangements, equal to doubled 2 layers disks setup.

While on the previous figures, each subsequent anti-peak was deeper than the previous (except of a single highest frequency anti-peak on the Figure 13 lower left picture, describing the situation with the 3-layer open-circuited system), the pattern is broken with the 4-layer disk tabs. The magnitude of the anti-peaks is lesser than in the 3-layer system, and it starts to decrease after the frequency of about 5 GHz.

4.2.2 Resonant Frequencies

In this section, the effects of adding the extra segments of coaxial transmission line between the CNT-covered tab and the short circuiter will be investigated.

Since the short-circuiting and open-circuiting the line causes the anti-peaks to invert with peaks (Multilayer Reflection part), they are caused by the destructive interference of the reflected waves. In order to check, in which part of the coaxial line the destructive interference happens, the extra segments were inserted in the part before, and then after the disk tabs. Changing the length of the involved segment should cause the resonant frequencies to change.

The addition of the extra segments to the coaxial line before the CNT-covered disk tab did not show up on the network analyzer screen. In contrary, extending the length of the coaxial line between the disk tab and before the short/open circuiter, caused the immediate change in number and distance of the pikes and anti-pikes, Figure 15:

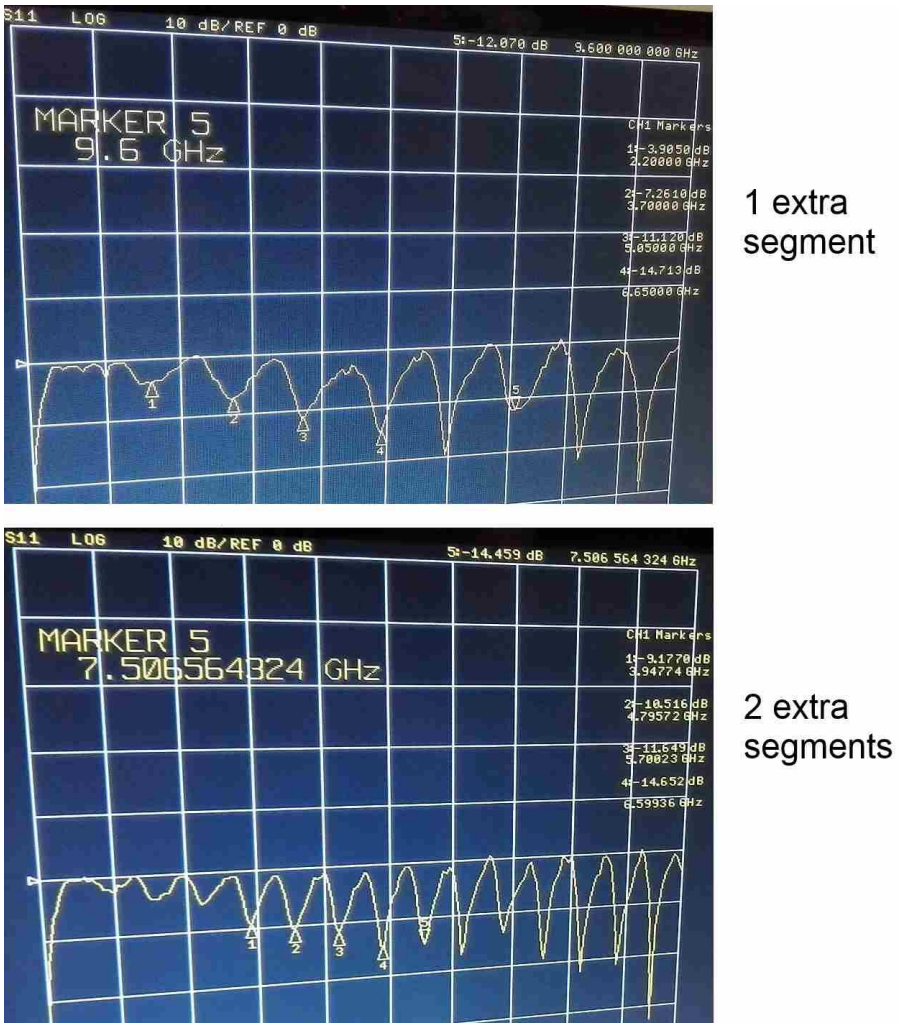

Figure 15. The effect of extending the length of the coaxial line part between the CNT-covered tab disk and the short circuiter on the RL waveform, the number and distance of the anti-peaks.

As it can be seen from the Figure 15 and from the comparison of it to the original 2-layer disk reflection shown in Figure 13, the distance between disks in terms of frequency, decreases. Averaging the distance between the anti-pikes and connecting it to the measured length of the coaxial line from the sample disk to the short-circuiter, Table 1 is produced:

Table 2. The relation between the length of the coaxial line from the CNT-covered disk sample installed across the coaxial line and the short-circuited or open-circuited end of the line.

Length [cm]	3	7	8	12	14	18
Frequency [GHz]	4,1	1,9	1,5	1,1	0,8	0,7

Based on the Table 2 data, the inverse relation between the length and the frequency can be found, Figure 16:

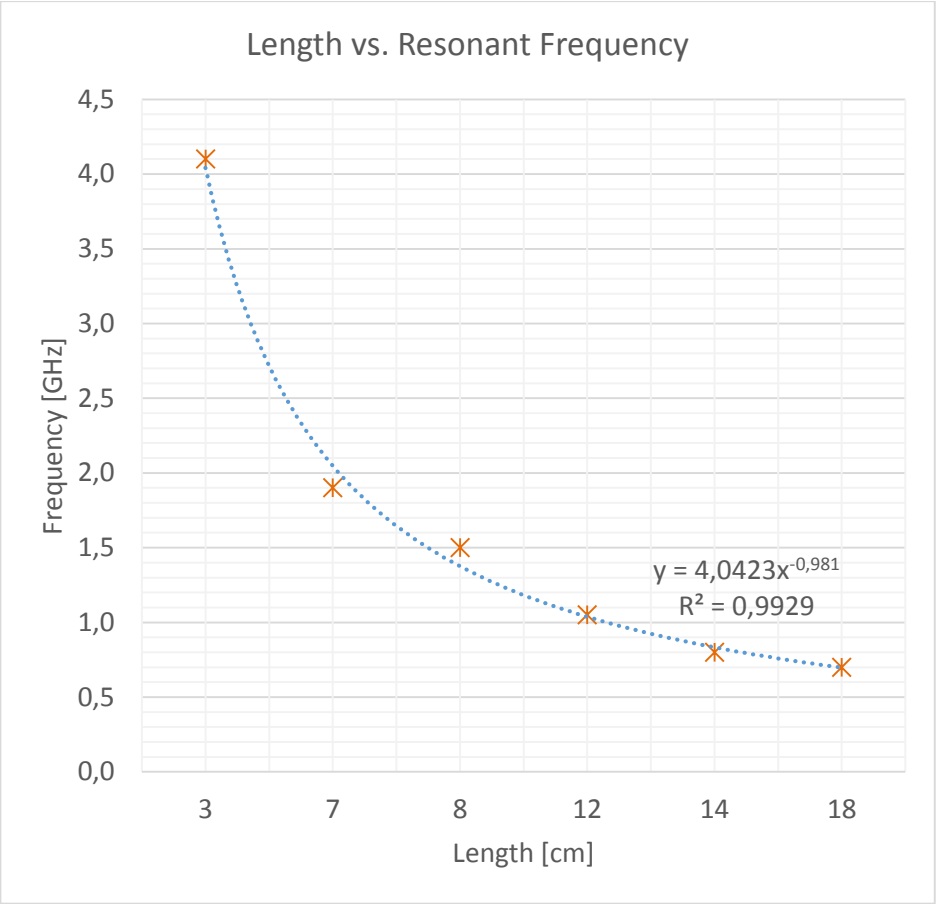

Figure 16. The plotted last part coaxial line length vs. measured resonance frequency (orange markers). The blue dotted best fit line with the best fit equation $y=4.0423x^{-0.981}$ and the coefficient of determination $R^2 = 0,9929$

As it can be seen from the Figure 16, the measured length has almost an inverse relation with the frequency, proving that the attenuation of the incident wave is caused by the destructive interference at resonant frequencies in the CNT-covered disk – short circuiter part of the coaxial line.

Combining with the information from the CNT-covered disk tab in coaxial cable behavior part, it can be concluded that the CNT-covered disk tab acts as the semi-permeable reflector and facilitates the destructive interference of the passed radiation. When the disk tab consists only of one CNT-based layer, it passes almost all radiation and the effect of the destructive interference between the transmitted and reflected radiation is small. However, when the disks tab becomes too thick and reflective, not enough radiation passes through to experience the destructive interference. The maximum attenuation of the incident plane wave radiation is found with the 3 layers CNT-covered disk tab.

4.3 Moving Sample Relative to Coaxial Cable

The measured return loss RL of three different samples at three different frequencies after moving sample from the center to different sides is shown in Figure 17:

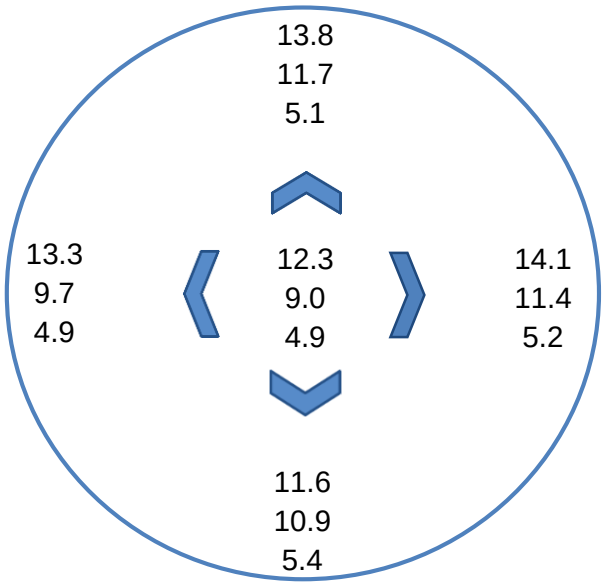

Figure 17. RL of centered and shifted sample.

The percentage difference from origin is summarized in Table 3:

Table 3. The absolute value of return loss and the percentage differences depending on the position of the sample.

#1	center	right	left	top	bottom
RL	12,3	14,1	13,3	13,8	11,6
% dev	0%	15%	8%	12%	6%
#2	center	right	left	top	bottom
RL	9,0	11,4	9,7	11,7	10,9
% dev	0%	27%	8%	30%	21%
#3	center	right	left	top	bottom
RL	4,9	5,2	4,9	5,1	5,4
% dev	0%	6%	0%	4%	10%

From Table 3 it can be seen that the deviation can be as high as 30%. It is a high value and, therefore, the deviations in measured parameters in terms of one CNT-covered sheet can come purely out of the dispositioning of the measured sample – similar magnitude of deviations can be observed from the raw measured date, Appendix 3 and 4. Consequently, the main experiment used 8 measurements per sheet in order to compensate the differences.

4.4 Corbino Disk Reflectometry Measurements

4.4.1 Samples RL Comparison

The measured reflection loss RL in the Corbino disk setup describes the shielding effectiveness of the metallic object covered with the CNT-based layer, Figure 18:

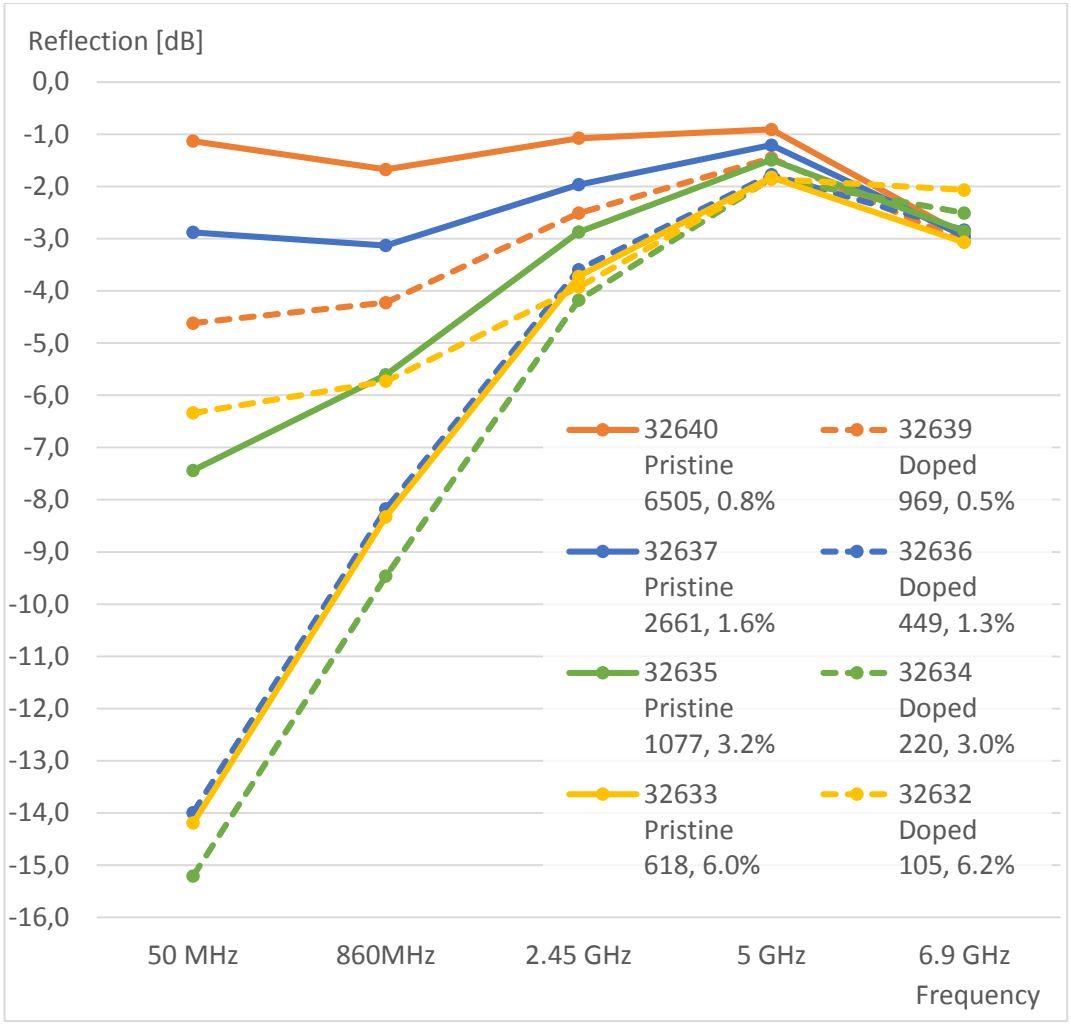

Figure 18. The amplitude of the return loss with respect to frequency. The solid lines represent the effect from the pristine layer cover, the dotted – doped CNT-based cover. The legend contains the information on the DC Ω/□ resistance and the optical absorption in percent.

It can be seen from Figure 18 that the thicker and more conductive CNT-based layers serve as a better covering material compared to the thinner ones. The tends to increase the shielding effectiveness (red, orange and green curves), however, in the case with the thickest CNT-covered sample, the situation inverts (yellow curve).

4.4.2 CNT-Covered Film Surface Impedance Z_s

The trend curve fitting program was employed in order to fit the 4th order polynomial curves to the found surface impedance Z_s, Figure 19:

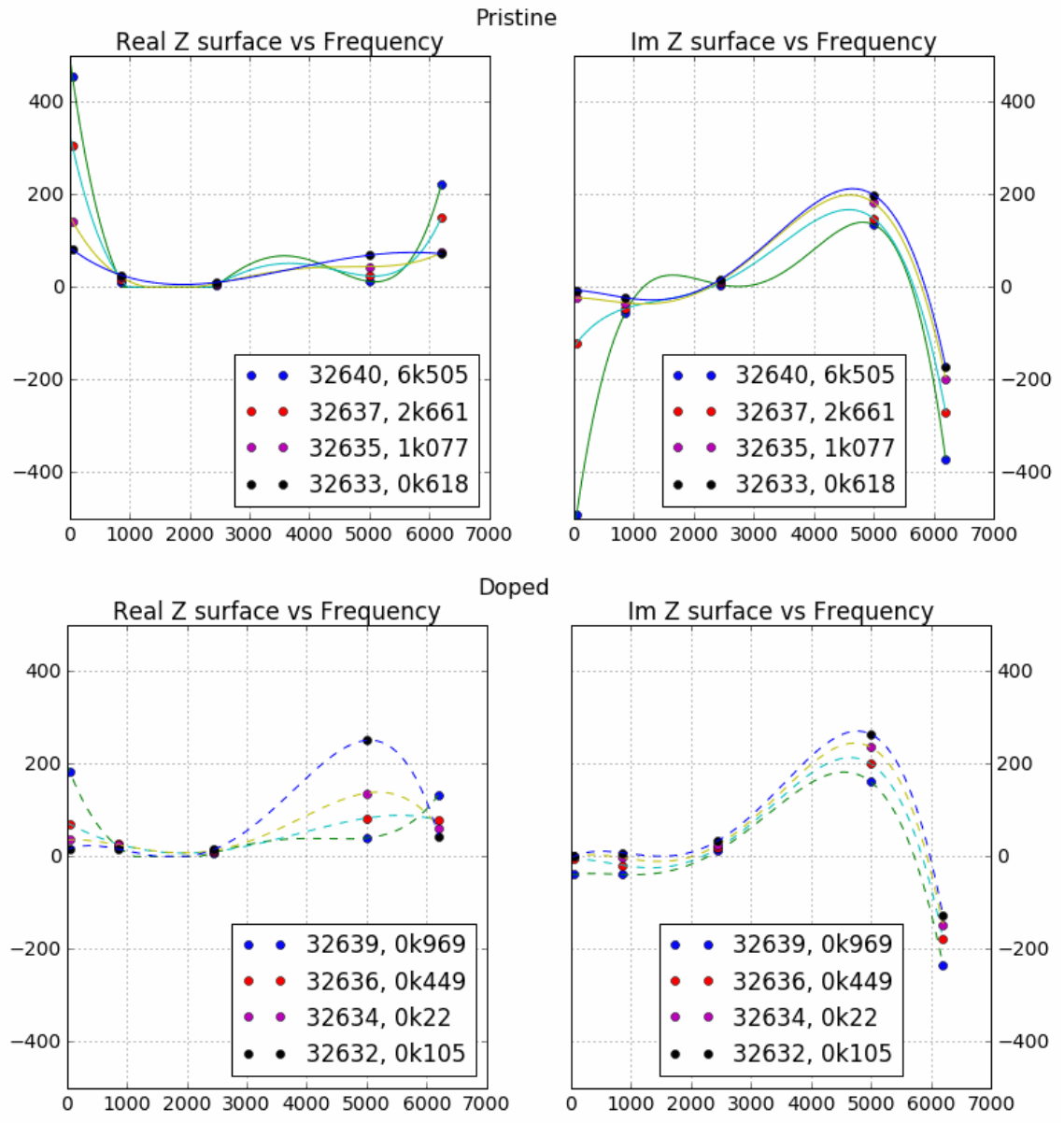

Figure 19. The complex surface impedance for the pristine and doped samples. The y-axis is the impedance in Ω, the x-axis is the frequency. The results for the pristine samples are in the top two pictures, for the doped – in the bottom. On the right pictures, the real part of the complex impedance is plotted, on the left pictures – the imaginary part. 4th order polynomial curves are fitted through the points at 5 target frequencies.

The samples with the subsequent DC resistance are located in either the same or inversed order in the complex $Z_s(\omega)$. For example, the real impedance of the doped sample (lower right picture) at 5 GHz has the pattern black-purple-orange-blue markers, which

is the inverse of the subsequent DC resistances, denoted as blue-orange-purple-black markers for the 969 Ω/□, 449 Ω/□, 220 Ω/□, 105 Ω/□ samples. This opens the possibility to predict the frequency-related parameters knowing just the DC resistance measurement and the type of production technology used.

4.4.3 CNT-Covered Film Complex Conductivity σ

The same program was used to fit the values for the complex conductivity, Figure 20:

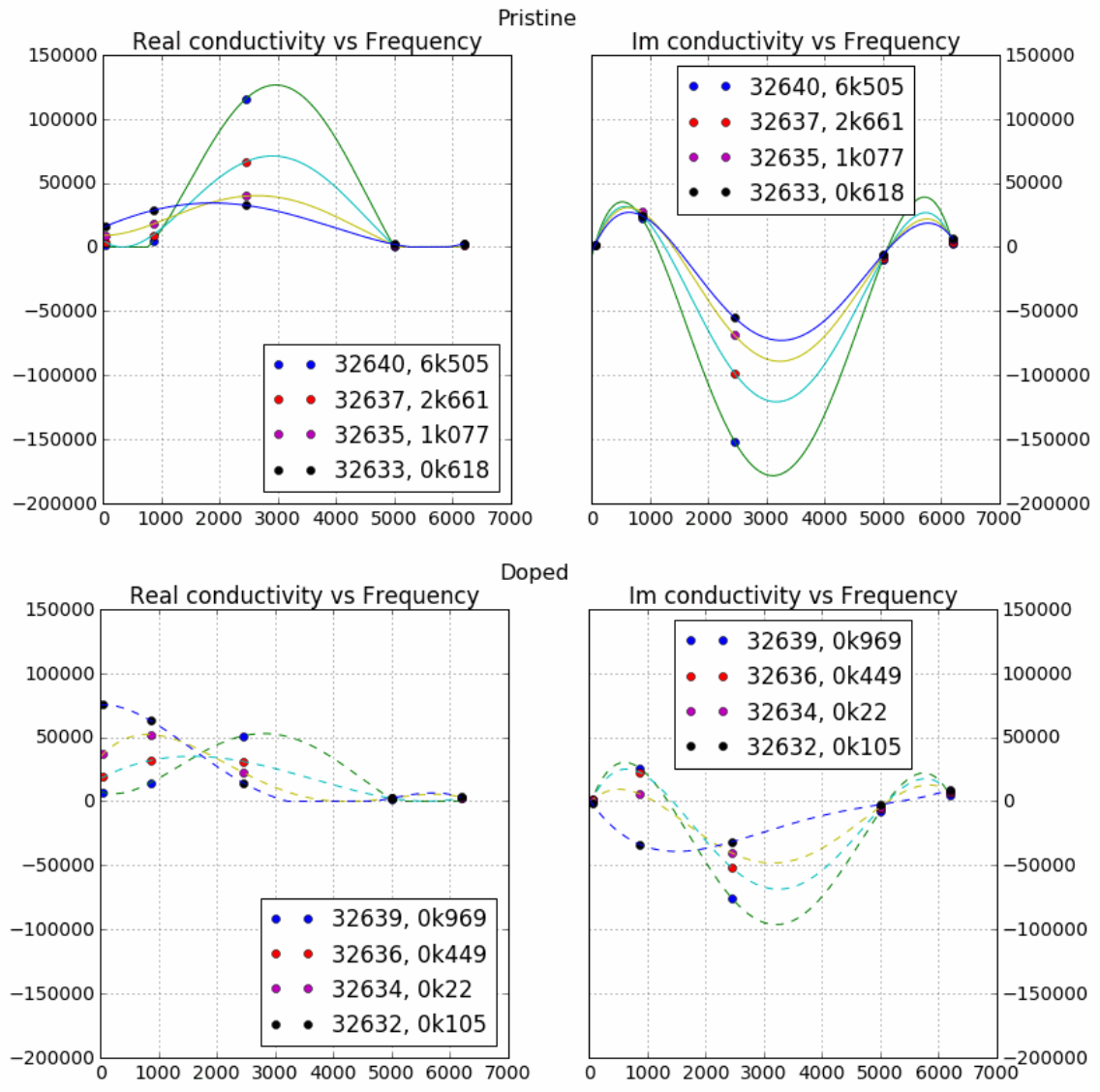

Figure 20. The complex conductivity of the samples with respect to frequency.

The principle of predicting the complex σ(ω) using the DC resistance works here as well.

The conductivity of the pristine samples experiences the raise in the 2.45 GHz region.

5 Discussion

The complex propagation constant can be deduced from the conductivity, as described by the equation (34). Knowing the conductivity and the complex propagation constant, every important frequency-dependent parameter, including the permeability μ and permittivity ε, can be deduced using the set of equations on the page [3, p23]. The deduced frequency-dependent parameters can then be used for the simulation and high frequency design.

The network analyzer with the function to save the data to digital form is preferably used in the future research to avoid the manual and limited measured data digitalization.

Keeping the CNT-covered film on a small distance from the highly conductive object causes the partial reflection, partial transmission and subsequent destructive/constructive interference. With the knowledge of the incident radiation frequency, the destructive interference worth of 20-30dB can be achieved, Figure 13. The multilayer structures with CNT-based layers one over another at different distances is one of the branches of the potential research.

Tightly covering of the highly conductive object with the CNT-based film has close to zero shielding effectiveness in starting from 1GHz and at least up to 13GHz range. However, the region below 50MHz looks interesting and may be additionally investigated (Figure 18).

6 Conclusions

6.1 Methods

The ‘innovative’ clutch-based device assembled for the Corbino disk experiment proved to be useful in terms of creating the good electrical connection between the coaxial line conductors and the Corbino disk electrodes, as well as the speed of sample changing.

The differences between the Corbino disks after the manual silver paste application and the manual positioning of the samples in the clutch device were considerable and several Corbino disk samples had to be used to eliminate these random errors. The magnitude of the random errors was lesser than the difference between the CNT-covered sheets.

6.2 Results

6.2.1 CNT-Covered Disk in Coaxial Cable Behaviour

Combining with the information from the CNT-covered disk tab in coaxial cable behavior part, it can be concluded that the CNT-covered disk acts as the semi-permeable reflector and facilitates the destructive interference of the transmitted radiation. When the disk tab consists only of one CNT-based layer, it passes almost all radiation and the effect of the destructive interference between the transmitted and reflected radiation is small. However, when the disks tab becomes too thick and reflective, not enough radiation passes through to experience the destructive interference. The maximum attenuation of the incident plane wave radiation is found with the 3 layers CNT-covered disks.

6.2.2 Corbino Disk Reflectometry

Using the Corbino disk setup, the values for the complex load impedance Z_L for the five frequencies of 50 MHz, 860 MHz, 2.45 GHz, 5 GHz and 6.2 GHz were measured. Using the measured Z_L, the values for the complex frequency-dependent surface impedance Z_s and conductivity σ at the corresponding frequencies were calculated and the trend curve plotted.

The correlation between the DC Ω/□ resistance and the complex frequency-dependent parameters was found, thus providing the way of prediction of the frequency-dependent behavior of the samples produced with the similar technology (pristine and doped samples behave differently).

The way to deduce the rest of the frequency-dependent parameters, using the values of the conductivity and complex propagation constant (34) through the set of equations from the book [4, p.23] was shown. The frequency-dependent parameters then may be plugged into the simulations and generally used for the high frequency design.

7 Acknowledgements

I would like to express the gratitude to Aarne Klementti, Metropolia Hybrid Media Technology Group supervisor. Despite organizing the conditions and performing the administrative work for the ongoing projects, Aarne Klementti was actively establishing the network of contacts between universities, students and companies, which allowed to meet with the customer company and make the present work possible.

Voyantic Oy kindly allowed the first RFID with the partial CNT film antennas samples on their own laboratory equipment measurement. This initial test demonstrated the effect of the CNT film antennas on the RFID tag behavior, which induced the further research in the 800-1200 MHz and later 50 MHz – 13.5 GHz frequency ranges. Voyantic Oy provided the world-class RFID measurement Tagformance unit for use in Metropolia University and the preliminary experiments were conducted with the convenient and user-friendly equipment.

I would like to express my warmest gratitude to Matti Fischer as he took care of the work in the hard times, provided the deep technical inside and support in any manner. His qualified involvement allowed the work to be finalized in the complete form.

Finally, I would like to say the special thanks to the customer company specialists who provided the very decent feedback about the early versions of the Thesis and made it possible to apply the important changes to it.

8 References

[1] A. G. Nasibulin, A. S. Anisimov, P. V. Pikhitsa, H. Jiang, D. P. Brown, M. Choi, and E. I. Kauppinen, “Investigations of CoverBud formation,” *Chem. Phys. Lett.*, vol. 446, no. 1–3, pp. 109–114, 2007.

[2] X. Sun, M. Gao, C. Li, and Y. Wu, “Microwave Absorption Characteristics of Carbon Nanotubes,” D. S. Yellampalli, Ed. INTECH, pp. 265–278.

[3] S. D. Keller and A. I. Zaghloul, “Lightweight , Durable Army Antennas Using Carbon Nanotube Technology (Final Report),” no. January, 2013.

[4] M. Dressel, G. Gruener, and G. F. Bertsch, “Electrodynamics of Solids: Optical Properties of Electrons in Matter,” *Am. J. Phys.*, vol. 70, no. 12, p. 1269, 2002.

[5] “Dielectrics.” [Online]. Available: http://hyperphysics.phy-astr.gsu.edu/hbase/electric/dielec.html#c1. [Accessed: 17-May-2016].

[6] a Schönhals, “Dielectric spectroscopy on the dynamics of amorphous polymeric systems,” *Sta*, no. i, pp. 1–17, 1998.

[7] H. Kitano, T. Ohashi, and A. Maeda, “Broadband method for precise microwave spectroscopy of superconducting thin films near the critical temperature,” *Rev. Sci. Instrum.*, vol. 79, no. 7, pp. 5–10, 2008.

[8] H. Xu, S. M. Anlage, L. Hu, and G. Gruner, “Microwave shielding of transparent and conducting single-walled carbon nanotube films,” *Appl. Phys. Lett.*, vol. 90, no. 18, pp. 3–5, 2007.

Preliminary Experiments

The purpose of the preliminary experiments was to find a potentially fruitful and interesting for the CNT-covered films producing customer company research area.
The series of experiments, where the primary one bared its limitations and became a basis for the next one were conducted.

Appendix does not include a complete description of the used theoretical considerations, experimental setups, and the results analysis's. However, it was considered to be potentially interesting for the readers to follow up the succession line to the main Thesis research topic.

Partially Replacement of the UHF RIFD Tag Dipole Antennas

The idea of the first experiment was to replace the metal-based RFID antennas with the transparent CNT-covered films, Figure 1:

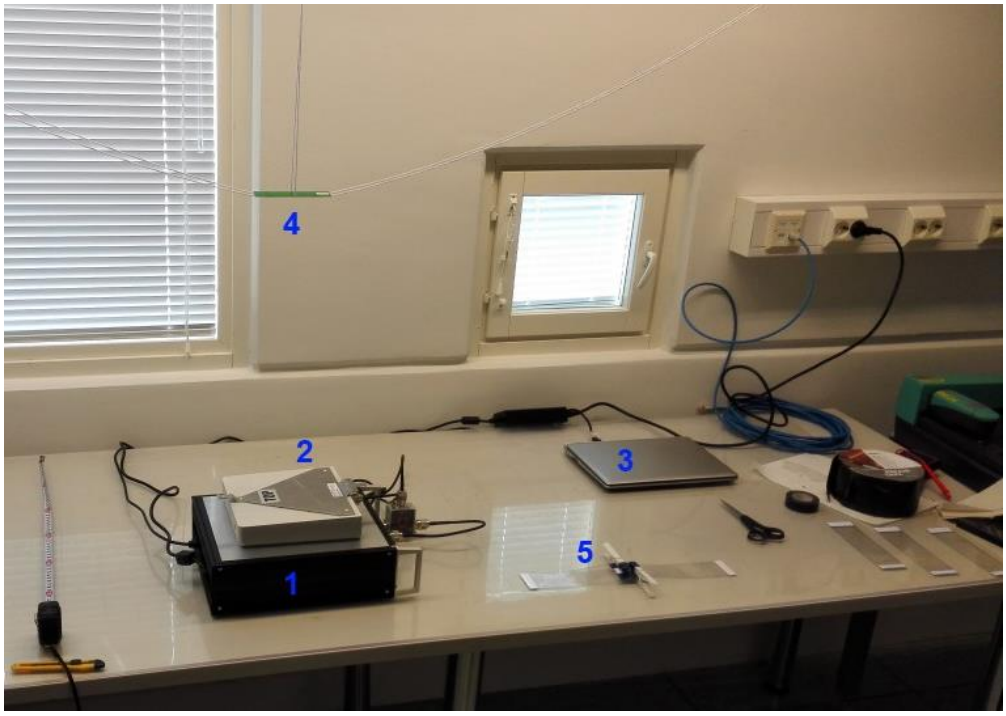

Figure 1 The RFID backscattered power measurement setup. (1) is the specialized Tagformance RFID measurement unit, which is connected to the (2) wideband 700 – 1200 MHz antenna and the (3) operator's PC. The reference wideband RFID tag (4) is located

50 cm from the antenna. The RFID chip with replaced dipole antennas (5) is waiting to be measured.
The structure of the RFID chip with the replacement antennas is shown in Figure 2:

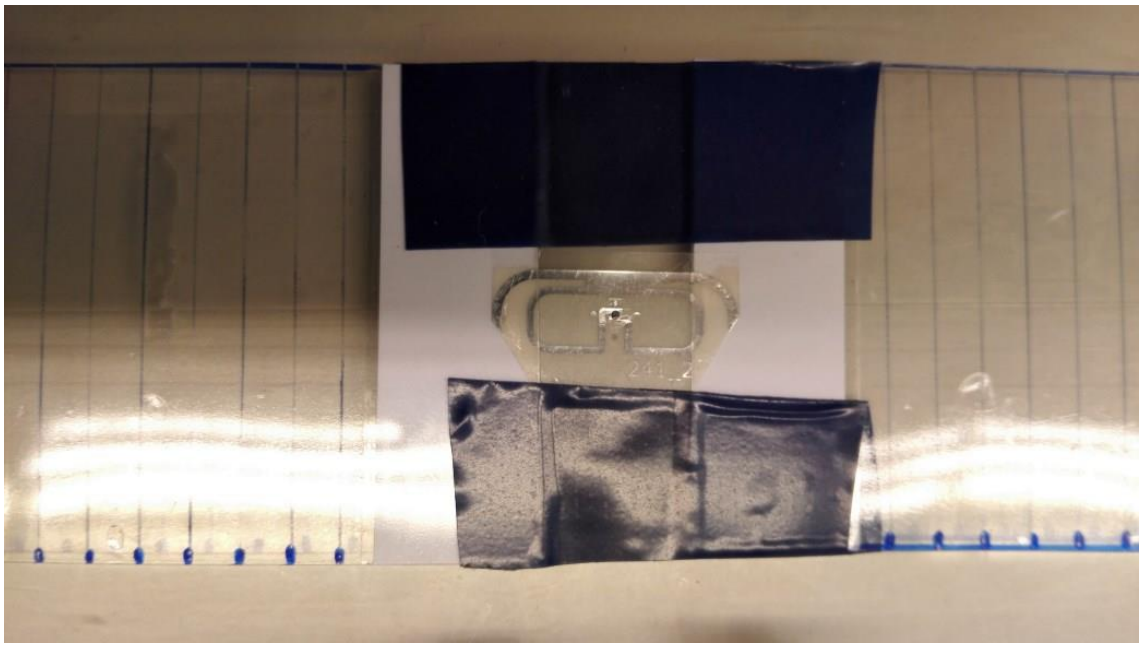

Figure 2. The RFID chip with replacement CNT-based antennas. The black dot in the centre is the RFID chip. It is connected to the rudimentary metal antennas. The metal antennas are attached to the conductive CNT layer deposited on the PET surface. The CNT-based antennas are laminated, however, in the connection areas, they are only covered with paper protectors to allow an access to make the metal – CNT interface.

In order to connect the RFID chip rudimentary metal antennas, they had to be first cleaned from the RFID covering protection plastics. For this purpose, the process of protection plastic removal was developed.

At first, the plastic was scratched with sand paper. The scratches had to be deep enough to penetrate to the glue layer between plastic and metal, and gentle enough not to harm the metal. The scratch damages allowed to wipe off the plastic protection layer with some harder material, e.g. plastic card plastic, since the scratched protective layer was likely to be pried off.

Despite some effect of the CNT-covered replacement antennas on the power received by an RFID tag, the number of variables in the experimental setup was too high e.g.:

- The length of the CNT-based antenna
- The width of the CNT-based antenna
- The length of rudimentary metallic antennas
- The form of metallic connection pads of the rudimentary metallic antennas
- The position of the connection point between the metallic and the CNT-based antenna

The number of variables associated with simultaneous CNT-based antenna modification and the rudimentary metallic antenna modification caused by the insufficient precision of manual operations, lead to the conclusion that the specialised study of the CNT-covered films as antennas without the effects from the RFID tag is required.

Dipole and patch 2.45 GHz antennas

The separate experiments of the simple dipole and patch antenna made out of the CNT-covered film antennas were performed, Figures 3 and 4:

Figure 3. The CNT-covered film dipole antenna connected to the network analyser.

The experiments demonstrated that the CNT-covered film antennas behaviour is significantly different from the expected metallic antennas behaviour for the selected dimensions.

That observation led to the fact that the frequency-dependent parameters of the CNT-covered film material should be studied in order to allow the modelling and subsequent frequency-related applications design.

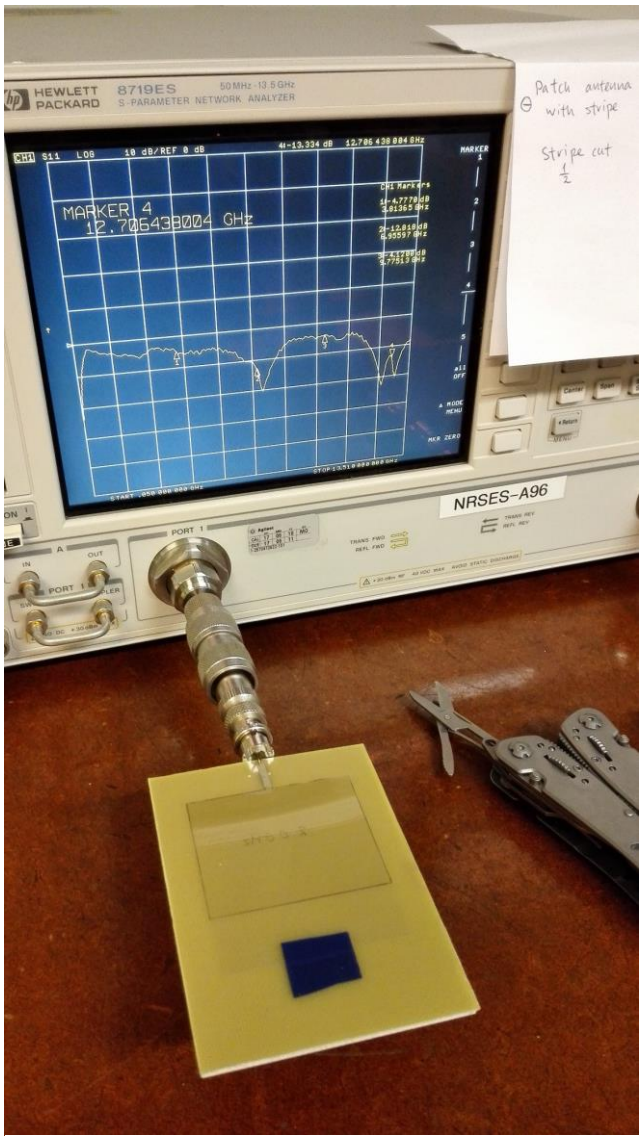

Figure 4. CNT-covered film cut in the form of the patch antenna located on top of the 1-sided printed circuit board (PCB) blank. The PCB copper layer from the other side, is connected to the coaxial cable outer conductor. The microstrip line leading to the rectangular body of the antenna is covered with the highly conductive silver nano paste and has the theoretical impedance of 50 Ω.

Source code of the polynomial fitting and plotting program

The program was run using Spyder 2.3.8 program with Python 3.5.1 64bits, Qt 4.8.7, PyQt4 (API v2) 4.11.4 on Windows 7 64 bit system.

```
import numpy as np
import matplotlib.pyplot as plt
import csv
from pylab import polyfit, polyval, plot

# Resistive and reactive components
R = []
X = []

# Storage for R + Xj curves deduced coefficients
Rm = []
Xm = []

# Read the file with measurements and fill R and X with values
with open('cond.csv', "rt", newline='') as cond:
    reader = csv.reader(cond, delimiter='\t')
    listC = list(reader)
    listC = [[int(float(j.replace(',','.'))) for j in i] for i in
listC]
    for row in listC:
        # 50MHz 860MHz 2.45GHz 5GHz 6.2GHz
        # a jb
        # 1 2   3 4    5 6     7 8  9 10
        R.append([row[0],   row[1],   row[3],   row[5],   row[7],
row[9]])
        X.append([row[0],   row[2],   row[4],   row[6],   row[8],
row[10]])

#print(R) Debug
#print(X) Debug

# Measurement frequencies, MHz
freq = [50, 860, 2450, 5000, 6200]


####
#Curve fit
####


length = len(R)
for i in range(length):
    Rm.append(polyfit(freq, R[i][1:7], 4))

length = len(X)
for i in range(length):
    Xm.append(polyfit(freq, X[i][1:7], 4))
```

```
####
#Plotting
####

WL = [12,6]
plt.rcParams.update({'font.size': 14})

x = np.arange(0,6200,5)

# 1) Pristine
pristineFig = plt.figure(1, figsize=(WL[0],WL[1]))
plt.suptitle('Pristine', fontsize=16)

pristineN = np.arange(0, 7, 2)

pristineSub1 = plt.subplot(121)
for i in pristineN:

    plt.plot(freq, R[i][1:7], 'o', label=str(R[i][0]))

    plotModel = polyval(Rm[i], x)
    plotModel = plotModel.clip(min=0)

    plot(x, plotModel)

plt.title('Real conductivity vs Frequency')
plt.ylim(-200000,150000)
plt.grid(True)
plt.legend(loc=4)

pristineSub2 = plt.subplot(122)
for i in pristineN:

    plt.plot(freq, X[i][1:7], 'o', label=str(X[i][0]))

    plotModel = polyval(Xm[i], x)

    plot(x, plotModel)

plt.title('Im conductivity vs Frequency')
plt.ylim(-200000,150000)
pristineSub2.yaxis.tick_right()
plt.grid(True)
plt.legend(loc=9)

plt.show()

# Plotting
# 2) Doped
dopedFig = plt.figure(1, figsize=(WL[0],WL[1]))
plt.suptitle('Doped', fontsize=16)

dopedN = np.arange(1, 8, 2)
```

```
dopedSub1 = plt.subplot(121)
for i in dopedN:

    plt.plot(freq, R[i][1:7], 'o', label=str(R[i][0]))

    plotModel = polyval(Rm[i], x)
    plotModel = plotModel.clip(min=0)

    plot(x, plotModel, ls='--')

plt.title('Real conductivity vs Frequency')
plt.ylim(-200000,150000)
plt.grid(True)
plt.legend(loc=4)

dopedSub2 = plt.subplot(122)
for i in dopedN:

    plt.plot(freq, X[i][1:7], 'o', label=str(X[i][0]))

    plotModel = polyval(Xm[i], x)

    plot(x, plotModel, ls='--')

plt.title('Im conductivity vs Frequency')
plt.ylim(-200000,150000)
dopedSub2.yaxis.tick_right()
plt.grid(True)
plt.legend()

plt.show()
```

Data in the `'cond.csv'` file:

32640	1343,7	1449,6	4651,5	22434,6	115489,2	-151691,1	906,9	-9814,8
1268,5	2802,6	6505						
32639	6928,6	1487,8	14346,0	26100,2	50996,3	-75644,4	1977,6	-7829,4
2356,7	4273,2	969						
32637	3770,2	1485,4	9364,7	24900,6	66551,6	-98425,2	1425,7	-8755,2
2071,8	3767,3	2661						
32636	18824,4	1328,1	31839,4	22650,4	31121,1	-51997,6	2380,9	-5741,8
2661,1	6363,9	449						
32635	9075,1	1495,2	17866,1	27253,3	39752,8	-68844,4	1711,3	-6905,4
2151,3	5848,6	1077						
32634	36940,7	702,0	52109,3	5926,7	22492,2	-40388,6	2475,2	-4220,9
3116,8	7548,2	220						
32633	16241,3	1380,3	28594,5	24426,1	32549,3	-55148,9	2118,2	-5976,4
2676,3	6480,6	618						
32632	75357,0	-2025,8	63020,7	-33470,1	14545,2	-31743,3	2511,0	-2637,9
3195,6	9255,1	105						

The raw measured return loss from the Corbino disk setup

The first column contains the sheet number and the measurement number for this sheet. For example, in the first table, sheet 1 is measured 8 times.

Columns 2-6 contain the values of the return loss for at the different frequencies in [dB]

The last three rows contain the

1. Averaged return loss of the 8 measurements
2. Standard deviation in [dB]
3. Standard deviation relation to the averaged return loss, expressed in percent

#32640	50 MHz	860MHz	2.45 GHz	5 GHz	6.9 GHz
Sh.1 1	-1,07	-1,73	-1,18	-0,97	-3,09
Sh.1 2	-1,08	-1,42	-0,84	-0,82	-2,88
Sh.1 3	-1,10	-1,62	-1,06	-0,94	-3,05
Sh.1 4	-1,19	-1,74	-1,04	-0,84	-2,72
Sh.1 5	-1,05	-1,49	-0,88	-0,79	-2,77
Sh.1 6	-1,22	-1,89	-1,44	-1,16	-3,36
Sh.1 7	-1,13	-1,69	-1,13	-0,96	-3,14
Sh.1 8	-1,21	-1,82	-1,04	-0,78	-2,45
average	-1,131	-1,675	-1,076	-0,908	-2,933
stdev	0,063	0,149	0,174	0,119	0,267
stdev(%)	5,5%	8,9%	16,2%	13,1%	9,1%

#32639	50 MHz	860MHz	2.45 GHz	5 GHz	6.9 GHz
Sh.2 1	-4,06	-3,79	-2,34	-1,42	-3,02
Sh.2 2	-4,56	-3,88	-2,09	-1,21	-2,71
Sh.2 3	-4,67	-4,23	-2,47	-1,41	-2,98
Sh.2 4	-4,53	-4,23	-2,64	-1,56	-3,18
Sh.2 5	-4,97	-4,23	-2,17	-1,18	-2,60
Sh.2 6	-4,96	-4,66	-2,89	-1,66	-3,29
Sh.2 7	-4,41	-4,05	-2,40	-1,39	-3,09
Sh.2 8	-4,78	-4,73	-3,09	-1,82	-3,58
average	-4,618	-4,225	-2,511	-1,456	-3,056
stdev	0,282	0,313	0,323	0,203	0,292
stdev(%)	6,1%	7,4%	12,8%	13,9%	9,5%

#32637	50 MHz	860MHz	2.45 GHz	5 GHz	6.9 GHz
Sh.3 1	-2,86	-3,20	-2,14	-1,35	-3,24
Sh.3 2	-2,95	-3,16	-1,97	-1,19	-2,96
Sh.3 3	-2,92	-3,15	-1,96	-1,21	-2,82
Sh.3 4	-3,12	-3,38	-2,18	-1,34	-3,04
Sh.3 5	-2,75	-3,08	-1,92	-1,17	-3,04

Sh.3 6	-2,71	-3,11	-2,08	-1,32	-3,19
Sh.3 7	-2,86	-3,04	-1,82	-1,08	-2,67
Sh.3 8	-2,86	-2,92	-1,66	-0,99	-2,67
average	-2,88	-3,13	-1,97	-1,21	-2,95
stdev	0,12	0,12	0,16	0,12	0,20
stdev(%)	4,1%	4,0%	8,2%	10,0%	6,9%

#32636	**50 MHz**	**860MHz**	**2.45 GHz**	**5 GHz**	**6.9 GHz**
Sh.4 1	-16,20	-8,48	-3,53	-1,69	-2,74
Sh.4 2	-13,04	-7,89	-3,56	-1,78	-2,89
Sh.4 3	-13,27	-7,77	-3,40	-1,71	-2,82
Sh.4 4	-16,64	-9,26	-4,03	-1,97	-2,95
Sh.4 5	-12,99	-7,85	-3,46	-1,69	-2,74
Sh.4 6	-14,96	-8,41	-3,55	-1,73	-2,69
Sh.4 7	-12,47	-8,02	-3,74	-1,91	-3,01
Sh.4 8	-12,38	-7,74	-3,47	-1,73	-2,85
average	-13,994	-8,178	-3,593	-1,776	-2,836
stdev	1,588	0,486	0,190	0,099	0,104
stdev(%)	11,3%	5,9%	5,3%	5,6%	3,7%

#32635	**50 MHz**	**860MHz**	**2.45 GHz**	**5 GHz**	**6.9 GHz**
Sh.5 1	-7,15	-5,31	-2,65	-1,36	-2,76
Sh.5 2	-7,36	-5,48	-2,71	-1,39	-2,75
Sh.5 3	-7,13	-5,76	-3,29	-1,78	-3,41
Sh.5 4	-8,18	-5,77	-2,78	-1,42	-2,71
Sh.5 5	-6,81	-5,20	-2,56	-1,29	-2,60
Sh.5 6	-7,19	-5,70	-3,15	-1,68	-3,15
Sh.5 7	-7,57	-5,74	-2,96	-1,54	-2,81
Sh.5 8	-8,12	-5,91	-2,88	-1,46	-2,67
average	-7,439	-5,609	-2,873	-1,490	-2,858
stdev	0,457	0,234	0,235	0,156	0,259
stdev(%)	6,1%	4,2%	8,2%	10,5%	9,1%

#32634	**50 MHz**	**860MHz**	**2.45 GHz**	**5 GHz**	**6.9 GHz**
Sh.6 1	-16,25	-9,76	-4,19	-1,83	-2,50
Sh.6 2	-16,96	-10,41	-4,77	-2,24	-2,87
Sh.6 3	-17,34	-9,69	-4,13	-1,84	-2,53
Sh.6 4	-15,46	-9,36	-4,02	-1,82	-2,41
Sh.6 5	-12,91	-8,67	-4,00	-1,63	-2,44
Sh.6 6	-13,12	-8,54	-3,62	-1,49	-2,11
Sh.6 7	-14,63	-9,64	-4,44	-2,02	-2,68
Sh.6 8	-14,99	-9,65	-4,27	-1,88	-2,51
average	-15,208	-9,465	-4,180	-1,844	-2,506

stdev	1,532	0,569	0,316	0,212	0,204
stdev(%)	10,1%	6,0%	7,6%	11,5%	8,2%

#32633	**50 MHz**	**860MHz**	**2.45 GHz**	**5 GHz**	**6.9 GHz**
Sh.7 1	-12,49	-8,07	-3,88	-1,99	-3,21
Sh.7 2	-13,11	-8,56	-4,03	-2,03	-3,46
Sh.7 3	-14,29	-7,90	-3,24	-1,51	-2,60
Sh.7 4	-14,20	-8,99	-4,18	-2,02	-3,57
Sh.7 5	-14,92	-8,75	-3,93	-1,98	-3,08
Sh.7 6	-12,28	-8,10	-3,93	-1,97	-3,34
Sh.7 7	-13,65	-8,00	-3,50	-1,68	-2,94
Sh.7 8	-18,60	-8,25	-3,09	-1,40	-2,35
average	-14,193	-8,328	-3,723	-1,823	-3,069
stdev	1,870	0,368	0,370	0,238	0,395
stdev(%)	13,2%	4,4%	9,9%	13,1%	12,9%

#32632	**50 MHz**	**860MHz**	**2.45 GHz**	**5 GHz**	**6.9 GHz**
Sh.8 1	-5,98	-5,42	-3,72	-1,72	-1,90
Sh.8 2	-6,72	-5,95	-4,06	-1,92	
Sh.8 3	-6,93	-6,23	-4,14	-1,98	-2,26
Sh.8 4	-6,12	-5,54	-3,72	-1,68	-1,92
Sh.8 5	-6,28	-5,75	-4,08	-1,99	-2,20
Sh.8 6	-6,23	-5,62	-3,78	-1,72	-1,97
Sh.8 7	-6,06	-5,50	-3,78	-1,80	-2,04
Sh.8 8	-6,37	-5,83	-4,13	-2,04	-2,17
average	-6,336	-5,730	-3,926	-1,856	-2,066
stdev	0,309	0,251	0,179	0,133	0,134
stdev(%)	4,9%	4,4%	4,6%	7,2%	6,5%

The raw measured complex load impedance and phase from the Corbino disk setup

The table consists of 8 repeated segments, one for each measured sample.

Row 1 contains the number and code of the measured sample.

Row 2 contains the information about the frequency used, as well as the heading for the phase subsection of the table.

Row 3 in **columns 2-11** specifies the real and imaginary part of the measured load impedance.

Row 3 in **columns 12-16** contains the information about the frequency used during the phase measurement.

Rows 4-11 in **columns 2-11** contain the raw measured complex impedance in [dB].

Rows 4-11 in **columns 12-16** contain the raw measured phase angle in degrees.

The **pre-last row** contains the averaged data from 8 measurements.

The **last row** contains the relation of the standard deviation to the averaged values presented in percent.

Meas #	Sample 1, 32640														
	50MHz		860MHz		2.45GHz		5GHz		6.2GHz		phase				
	real	img	real	img	real	img	real	img	real	img	50MHz	860MHz	2.45GHz	5GHz	6,2GHz
1	435,8	-451,9	11,4	-53,2	3,7	7,8	13,3	146,5	142,6	-367,0	-6,4	-85,1	162,3	37,4	-13,5
2	458,1	-469,3	11,4	-53,3	3,7	7,7	12,7	145,5	147,0	-370,1	-6,6	-85,3	162,0	37,5	-13,3
3	480,8	-509,0	13,5	-62,4	4,4	2,3	13,4	113,2	672,3	-329,3	-5,9	-75,8	174,7	47,2	-3,4
4	463,2	-492,8	12,3	-57,6	3,8	5,3	12,0	131,0	174,9	-449,2	-6,3	-80,4	167,8	41,5	-11,0
5	441,5	-520,6	10,0	-55,1	3,0	7,5	9,8	148,3	109,5	-335,4	-6,3	-83,3	163,0	37,2	-15,3
6	455,7	-482,2	12,6	-57,8	4,3	5,0	15,7	130,2	163,4	-275,5	-6,3	-80,1	168,7	41,6	-15,3
7	494,5	-496,8	11,9	-60,3	3,5	4,1	9,8	123,9	314,0	-528,8	-5,8	-77,9	170,7	43,8	-8,0
8	419,9	-514,7	11,5	-55,0	3,6	6,8	11,1	141,4	63,0	-332,2	-6,8	-83,2	164,4	38,7	-16,5
avg	456,2	-492,2	11,8	-56,8	3,7	5,8	12,2	135,0	223,3	-373,4	-6,3	-81,4	166,7	40,6	-12,0
stdev	4,9%	4,5%	8,2%	5,5%	11,1%	32,1%	15,2%	8,7%	81,8%	20,0%	4,9%	3,9%	2,6%	8,3%	34,4%
Meas #	Sample 2, 32639														
	50MHz		860MHz		2.45GHz		5GHz		6.2GHz		phase				

	real	img	real	img	real	img	real	img	real	img	50MHz	860MHz	2.45GHz	5GHz	6,2GHz
1	200,3	-46,3	19,7	-40,6	6,8	12,4	36,7	173,2	86,8	-258,2	-6,7	-96,6	151,6	31,1	-19,7
2	190,8	-41,2	20,9	-40,8	7,2	11,9	35,8	154,5	114,6	-260,6	-6,5	-95,4	152,9	32,8	-18,2
3	199,3	-44,1	22,5	-42,5	8,2	9,8	34,8	144,1	179,4	-259,7	-6,4	-92,5	157,3	36,6	-14,9
4	180,8	-37,0	21,8	-39,5	8,2	11,8	40,7	156,1	163,4	-243,6					
5	163,2	-35,3	18,8	-33,4	6,8	16,4	44,4	206,4	69,1	-207,2	-7,8	-107,1	143,2	26,2	-24,6
6	171,9	-35,3	22,8	-38,0	8,8	12,0	43,2	156,0	130,6	-222,1	-7,1	-97,9	152,4	33,4	-19,2
7	196,3	-44,7	21,4	-40,2	8,1	11,4	38,1	154,8	136,8	-208,5	-6,7	-96,0	153,7	34,2	-19,2
8	169,4	-34,0	24,0	-38,3	9,6	11,2	46,2	143,2	191,0	-214,5	-7,0	-96,7	153,9	35,6	-15,0
avg	184,0	-39,7	21,5	-39,2	8,0	12,1	40,0	161,0	134,0	-234,3	-6,9	-97,4	152,2	32,9	-18,4
stdev	7,4%	11,5%	7,3%	6,5%	11,5%	14,6%	10,0%	11,9%	30,1%	9,5%	6,2%	4,1%	2,5%	9,1%	16,1%
Meas #	Sample 3, 32637														
	50MHz		860MHz		2.45GHz		5GHz		6.2GHz		phase				
	real	img	real	img	real	img	real	img	real	img	50MHz	860MHz	2.45GHz	5GHz	6,2GHz
1	305,8	-115,4	19,0	-49,4	6,6	7,3	23,0	134,0	204,0	-276,3	-6,4	-86,4	163,3	40,0	-13,4
2	300,0	-114,5	18,1	-46,8	6,4	9,1	25,5	146,4	127,2	-250,7	-6,7	-89,8	159,1	36,8	-18,1
3	316,3	-140,0	16,6	-45,8	5,9	10,0	24,5	155,6	119,8	-241,4	-6,8	-91,5	157,1	34,9	-18,9
4	268,2	-93,4	17,4	-42,6	6,5	11,4	29,5	160,5	132,1	-256,6	-6,8	-95,1	154,0	33,6	-17,6
5	316,9	-127,5	17,2	-46,8	5,9	9,3	22,0	150,5	146,0	-247,6	-6,5	-90,2	158,6	36,2	-17,1
6	316,0	-126,9	17,9	-48,0	6,3	9,3	23,5	140,5	199,2	-318,8	-6,5	-88,5	160,9	38,4	-12,9
7	310,3	-133,2	17,6	-47,5	6,3	8,7	24,1	144,2	151,8	-272,6	-6,5	-89,2	160,0	37,4	-16,0
8	307,3	-117,6	16,7	-46,9	5,6	9,4	20,3	152,0	132,1	-306,4	-6,7	-90,2	158,4	35,9	-15,7
avg	305,1	-121,1	17,6	-46,7	6,2	9,3	24,1	148,0	151,5	-271,3	-6,6	-90,1	158,9	36,6	-16,2
stdev	4,9%	11,1%	4,1%	4,0%	5,2%	11,7%	10,5%	5,4%	20,1%	9,8%	2,4%	2,6%	1,6%	5,1%	12,5%
Meas #	Sample 4, 32636														
	50MHz		860MHz		2.45GHz		5GHz		6.2GHz		phase				
	real	img	real	img	real	img	real	img	real	img	50MHz	860MHz	2.45GHz	5GHz	6,2GHz
1	64,6	-4,3	27,5	-17,4	11,4	19,8	89,4	207,0	72,5	-168,8	-13,5	-129,5	135,0	23,2	-28,3
2	60,7	-3,8	25,6	-15,6	10,4	22,1	108,6	240,0	49,5	-148,2	-18,2	-135,7	130,7	19,8	-34,1
3	70,6	-5,4	26,2	-19,5	10,6	20,2	90,6	214,3	57,0	-156,7	-11,8	-126,3	134,5	22,6	-31,7
4	63,8	-3,9	28,2	-17,5	11,4	19,3	83,9	202,1	78,4	-185,0	-13,5	-128,5	136,0	24,2	-26,0
5	68,9	-5,0	26,2	-19,1	10,1	20,2	84,6	224,2	52,0	-174,0	-12,7	-127,3	134,5	22,3	-29,8
6	78,2	-5,8	29,2	-23,2	11,6	16,6	70,2	175,2	99,7	-198,5	-9,1	-115,5	141,6	27,9	-23,0
7	82,0	-6,4	29,8	-24,5	11,9	15,5	67,6	155,4	120,0	-197,7	-8,4	-112,4	143,8	29,3	-21,1
8	78,0	-6,1	28,1	-22,8	11,1	17,4	71,7	185,4	97,2	-195,3	-9,7	-117,5	140,1	26,6	-23,5
avg	70,8	-5,1	27,6	-19,9	11,1	18,9	83,3	200,5	78,3	-178,0	-12,1	-124,1	137,0	24,5	-27,2
stdev	10,3%	18,7%	5,2%	14,9%	5,3%	10,9%	15,2%	12,8%	30,5%	10,1%	24,5%	6,1%	3,0%	12,3%	15,7%
Meas #	Sample 5, 32635														
	50MHz		860MHz		2.45GHz		5GHz		6.2GHz		phase				
	real	img	real	img	real	img	real	img	real	img	50MHz	860MHz	2.45GHz	5GHz	6,2GHz

1	159,8	-30,9	21,4	-35,1	8,1	14,0	44,7	180,4	66,2	-179,7	-7,2	-102,9	148,0	29,4	-27,7
2	130,6	-20,4	21,5	-31,7	7,6	16,5	47,8	205,6	49,7	-184,9	-7,7	-108,0	142,7	26,1	-28,5
3	161,8	-26,9	24,7	-39,8	9,0	10,4	38,7	146,7	127,3	-196,5	-6,2	-94,3	155,8	35,5	-20,5
4	139,7	-22,1	23,4	-34,8	8,7	13,8	45,5	170,5	96,5	-212,0	-7,1	-101,9	148,5	30,8	-22,2
5	146,1	-26,3	20,2	-32,7	7,1	16,3	42,3	208,3	46,9	-191,8	-7,7	-107,5	143,2	26,1	-27,8
6	132,6	-20,6	22,4	-32,0	8,5	15,6	51,5	186,9	72,2	-194,6	-7,6	-106,9	144,4	28,0	-25,6
7	145,7	-25,0	22,1	-33,9	8,0	14,6	42,5	183,4	80,1	-211,4	-7,5	-104,3	146,7	29,2	-23,5
8	129,3	-18,7	23,1	-33,2	8,0	15,1	45,3	180,6	64,1	-215,3	-7,4	-104,4	145,7	28,1	-24,2
avg	143,2	-23,9	22,3	-34,2	8,1	14,5	44,8	182,8	75,4	-198,3	-7,3	-103,8	146,9	29,1	-25,0
stdev	8,2%	16,2%	5,8%	7,1%	7,2%	12,4%	8,0%	10,0%	32,7%	6,3%	6,1%	4,0%	2,6%	9,7%	10,9%
Meas #	Sample 6, 32634														
	50MHz		860MHz		2.45GHz		5GHz		6.2GHz		phase				
	real	img	real	img	real	img	real	img	real	img	50MHz	860MHz	2.45GHz	5GHz	6,2GHz
1	37,7	-0,7	26,0	-4,0	14,0	24,2	129,7	226,6	65,2	-150,7	-175,7	-167,6	125,4	19,1	-31,6
2	39,2	-0,8	27,7	-4,4	15,6	22,8	123,7	187,3	86,5	-155,3	-175,0	-165,6	127,3	21,3	-28,1
3	35,5	-0,8	24,3	-2,9	13,0	25,8	140,2	258,1	49,8	-150,0	-176,2	-171,2	122,9	17,2	-33,7
4	40,0	-1,0	26,6	-5,2	14,2	23,7	128,1	208,0	75,5	-156,5	-173,3	-163,5	126,3	20,0	-29,4
5	34,3	-0,6	24,3	-1,7	14,1	25,6	140,0	245,2	62,5	-136,8	-177,1	-175,1	122,7	17,7	-34,2
6	34,5	-0,6	24,0	-2,3	13,1	26,1	143,9	261,9	51,9	-150,9					
7	32,9	-0,4	24,1	-1,1	14,0	26,2	148,4	243,9	57,8	-144,4	-178,0	-176,8	121,6	17,2	-33,8
8	34,3	-0,6	24,2	-2,2	13,1	26,0	143,3	261,6	50,7	-152,8	-177,3	-173,5	122,4	16,9	-33,2
avg	36,0	-0,7	25,1	-3,0	13,9	25,1	137,2	236,6	62,5	-149,7	-176,2	-170,8	123,9	18,3	-32,2
stdev	6,8%	23,8%	5,3%	45,0%	5,6%	4,9%	6,0%	10,8%	19,5%	4,0%	0,8%	2,6%	1,6%	8,5%	6,6%
Meas #	Sample 7, 32633														
	50MHz		860MHz		2.45GHz		5GHz		6.2GHz		phase				
	real	img	real	img	real	img	real	img	real	img	50MHz	860MHz	2.45GHz	5GHz	6,2GHz
1	85,1	-7,6	26,4	-24,0	10,3	17,8	69,7	195,7	70,6	-179,3	-9,2	-117,0	139,5	25,7	-27,3
2	88,2	-7,9	28,6	-25,4	11,3	15,6	66,2	172,3	96,6	-170,0	-8,4	-112,2	143,7	28,6	-25,6
3	76,3	-6,4	25,2	-21,2	9,4	19,9	73,0	227,7	46,7	-169,0	-10,8	-123,7	135,4	22,6	-31,0
4	83,0	-7,2	27,9	-23,3	11,2	16,7	69,2	183,8	79,5	-158,8	-9,4	-116,9	141,5	27,1	-28,7
5	74,5	-5,7	26,5	-21,2	10,0	19,1	72,3	211,9	61,0	-180,6	-10,5	-122,4	137,0	24,0	-28,2
6	86,1	-7,9	26,5	-24,0	10,6	17,6	69,2	192,8	75,9	-169,9	-9,1	-117,0	139,8	26,2	-27,9
7	88,4	-8,3	27,3	-25,2	10,7	16,4	63,7	181,1	93,2	-178,5	-8,5	-114,0	142,3	27,9	-25,1
8	70,9	-5,3	26,0	-19,9	9,7	20,0	75,7	226,4	55,3	-183,3	-11,5	-125,7	135,1	22,6	-28,1
avg	81,6	-7,0	26,8	-23,0	10,4	17,9	69,9	199,0	72,3	-173,7	-9,7	-118,6	139,3	25,6	-27,7
stdev	7,7%	14,9%	3,7%	8,3%	6,2%	8,5%	5,1%	9,8%	22,8%	4,4%	10,8%	3,8%	2,1%	8,3%	6,2%
Meas #	Sample 8, 32632														
	50MHz		860MHz		2.45GHz		5GHz		6.2GHz		phase				
	real	img	real	img	real	img	real	img	real	img	50MHz	860MHz	2.45GHz	5GHz	6,2GHz

1	18,1	0,4	16,8	8,4	15,6	34,0	241,0	265,2	45,0	-132,5	178,9	158,6	108,0	11,9	-37,8
2	17,5	0,4	16,0	8,6	15,3	34,9	261,4	278,4	40,5	-118,3	178,9	158,4	106,7	11,0	-42,1
3	18,9	0,4	17,4	8,0	16,0	33,6	239,2	241,7	48,7	-126,6	179,0	159,4	108,3	12,0	-38,6
4	17,6	0,5	16,5	8,7	15,9	34,4	248,1	257,8	43,7	-130,8	178,7	157,9	107,2	11,6	-38,5
5	17,7	0,5	16,7	8,9	16,6	34,3	233,4	284,6	49,8	-131,7	178,7	157,4	107,0	12,4	-37,2
6	16,5	0,5	15,4	9,1	14,8	35,5	277,8	291,8	36,7	-128,3	178,7	157,3	106,0	10,4	-40,0
7	16,9	0,5	15,9	9,1	15,8	35,1	257,5	250,5	44,5	-127,4	178,8	157,2	106,2	11,1	-39,0
8	17,7	0,5	16,6	8,7	16,6	34,5	250,6	244,9	45,4	-129,2	179,0	157,9	107,1	11,6	-38,5
avg	17,6	0,5	16,4	8,7	15,8	34,5	251,1	264,4	44,3	-128,1	178,8	158,0	107,1	11,5	-38,9
stdev	3,9%	10,0%	3,6%	4,0%	3,6%	1,7%	5,3%	6,7%	8,9%	3,3%	0,1%	0,4%	0,7%	5,2%	3,6%

The waveform comparison from the Corbino disk setup

The table of images consists of the colour-adjusted images of the network analyser screen for every sample sheet first measurement. The waveforms were rather similar for the measurements within the single sample, therefore, only one image per category per sample is used for the comparison.

The first image column shows the waveform of the reflection loss. The second – the phase of the reflected signal. The third – the complex load impedance on the Smith chart.

Sheet 1
32640

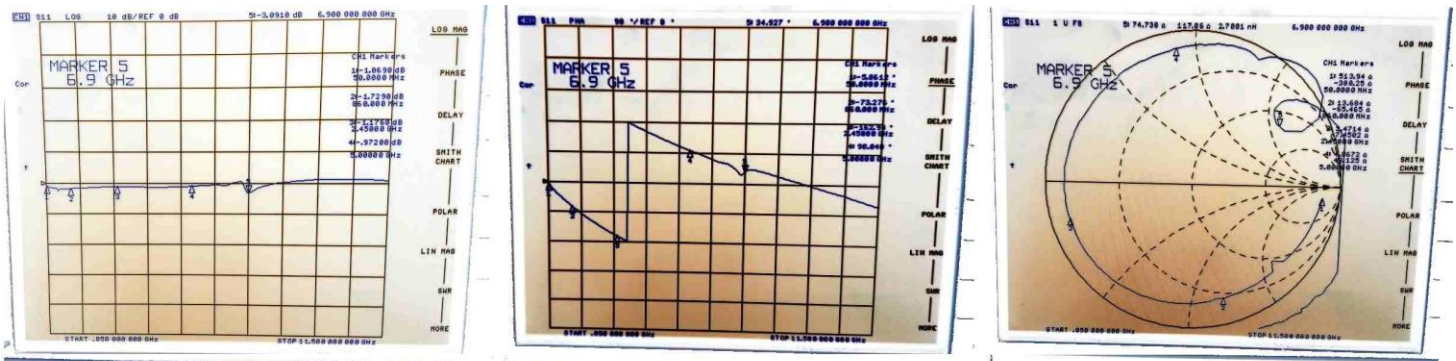

Sheet 2
32639

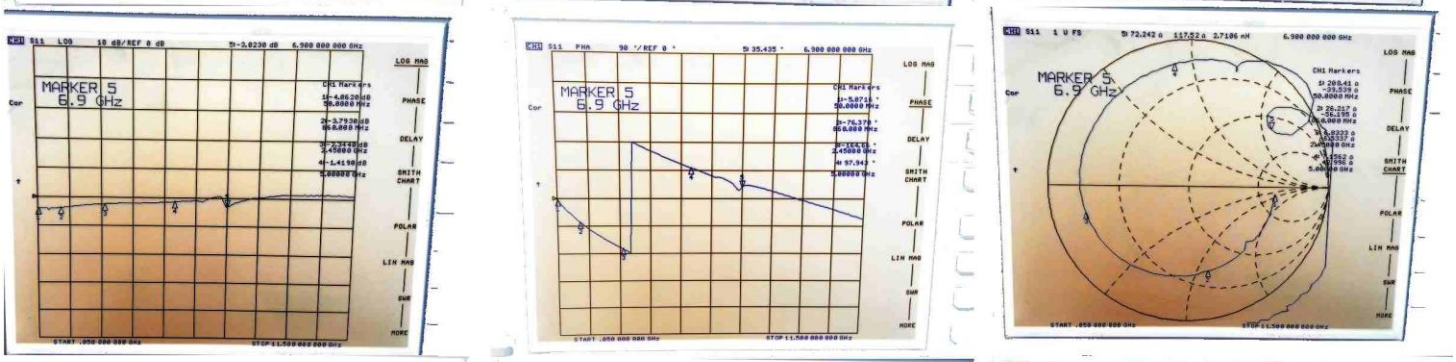

Sheet 3
32637

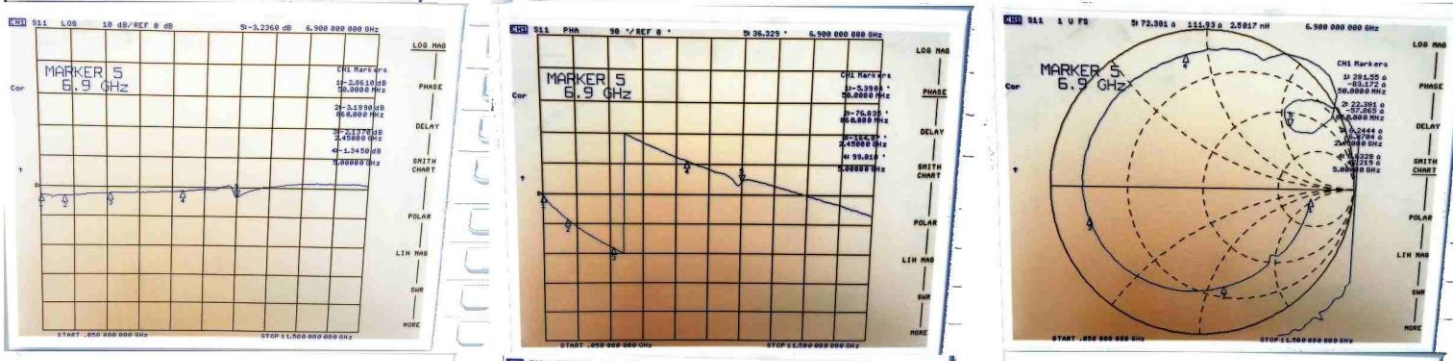

Sheet 4
32636

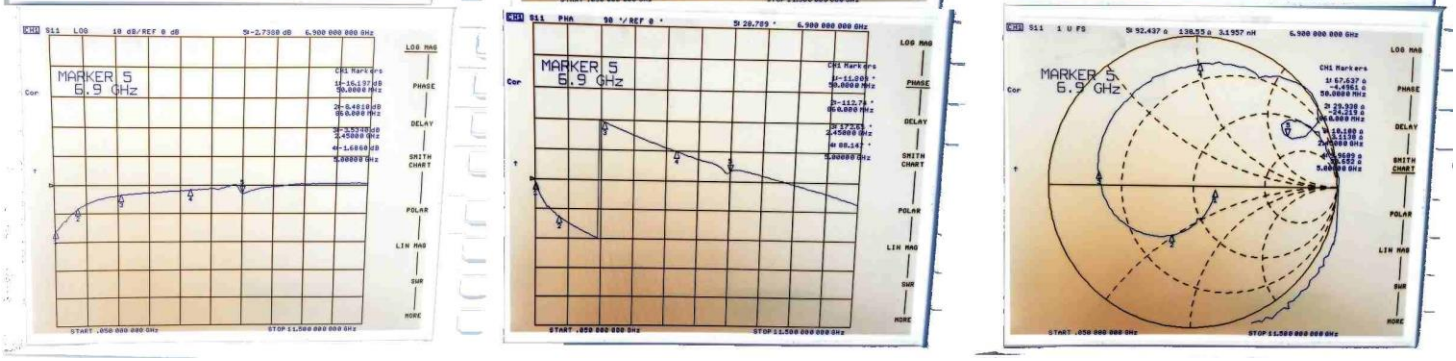

Sheet 5
32635

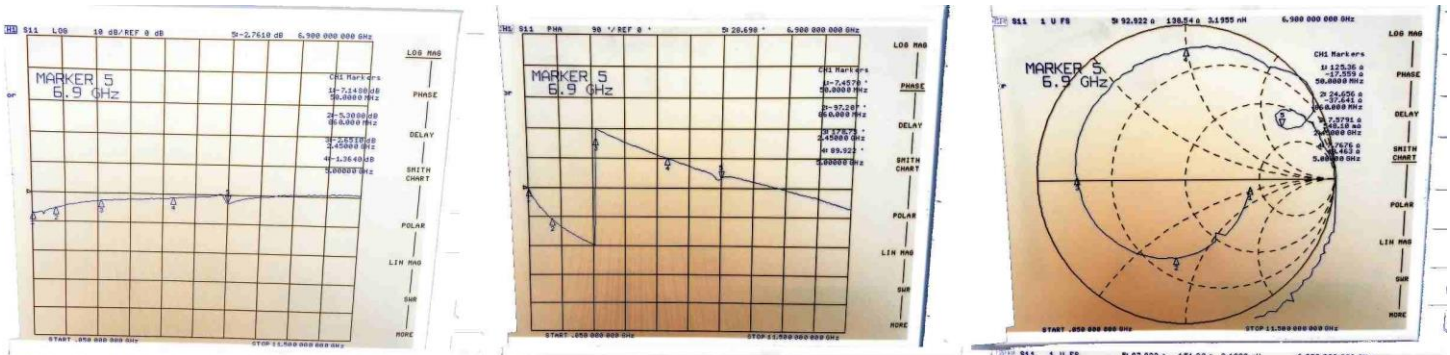

Sheet 6
32634

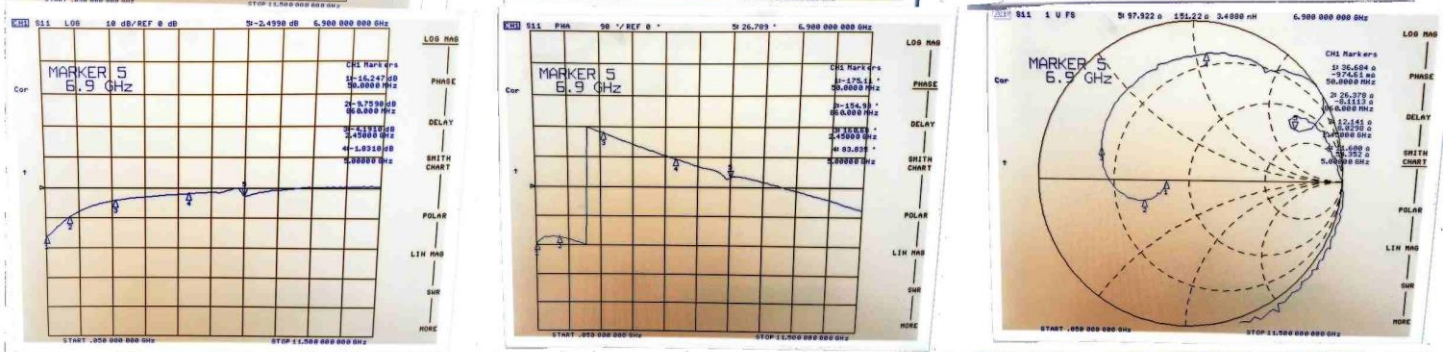

Sheet 7
32633

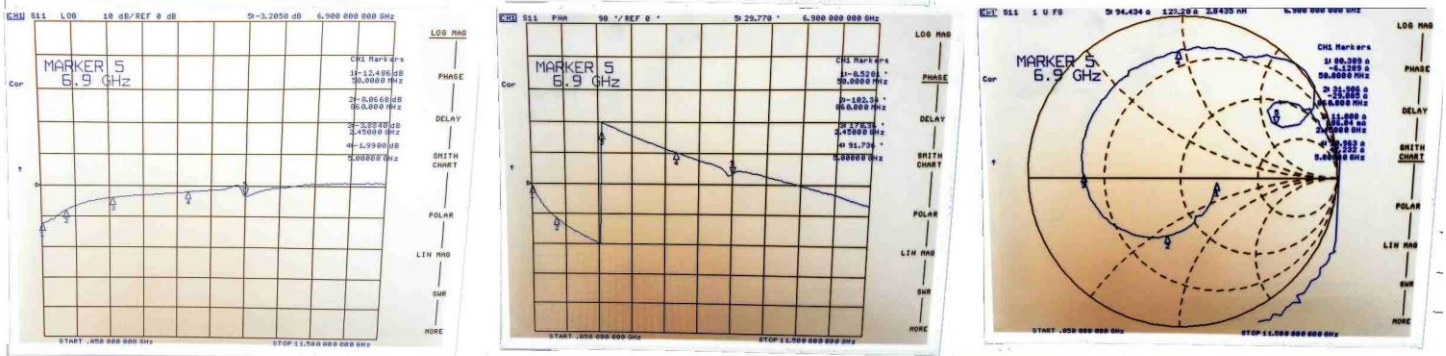

Sheet 8
32632